



Study for Detection of
Metallic Contaminant in Electrode of Lithium-ion Battery using
a Hall Probe



Master of Engineering
Department of Electrical and Electronic Information
اونيورسيتي مليسيا قهغ السلطان عبد الله
UNIVERSITI MALAYSIA PAHANG
AL-SULTAN ABDULLAH

ABDUL AZIM BIN JAIS

071302

PERPUSTAKAAN 6/1 P UNIVERSITI MALAYSIA PAHANG	
No. Perolehan 077660	No. Panggilan TK
Tarikh 23 AUG 2013	2945 L58 A95 2012

Thesis

Toyohashi University of Technology

電気・電子情報工学専攻	学籍番号	071302
申請者氏名	ABDUL AZIM BIN JAIS	

指導教員氏名	稲田亮史
--------	------

論文要旨(修士)

論文題目	ホール素子を用いたリチウムイオン電池用電極中の金属異物の検出に関する研究
------	--------------------------------------

携帯電話やノートパソコン等のモバイル端末用電源に使用されているリチウムイオン電池は、その高エネルギー密度性故に、内部短絡等の不具合が発生した場合には発火・破裂に至ることもあり、その安全性が社会問題化している。電池製造工程における電池部材中への金属異物の混入は内部短絡を引き起こす一因となるため、電池の製造段階にて早期に検出する必要がある。現在、高温超電導 SQUID を用いた電池部材中の混入金属異物検出に関する検討が進められており、 $50\mu\text{m}$ 程度の強磁性金属片を再現性良く検出できることが報告されているが、SQUID の駆動に冷媒もしくは冷凍機が必要なため、装置が大型かつ高価になるという問題がある。一方、より小型・安価で汎用性の高い磁界センサの一つにホール素子がある。ホール素子の磁界検出感度は SQUID よりも低いが、外部磁界を印加し電極中に混入した金属異物の発生磁界強度を増加させることで、金属異物の発生磁界を検出できる可能性がある。本研究では、ホール素子を用いてリチウムイオン電池用電極に混入した金属異物の磁界分布を測定し、より簡便かつ安価な金属異物検出技術としての適用可能性を検討することを目的とした。

Al箔上にコバルト酸リチウム (LiCoO_2) 正極材料を塗布した電極 ($15\text{mm}\times 15\text{mm}$, 厚さ 0.09mm) を作製し、この塗布電極に金属異物としてまず直径 $50\mu\text{m}$ 、長さ $0.5\text{--}2\text{mm}$ の鉄線を1個入れたものを試料とした。これをベークライト製の試料ホルダ上に固定し、試料面 ($x\text{-}y$ 面) 上で2次的にホール素子を走査させながら、試料面に垂直な方向 (z 方向) の磁界分布測定を行った。測定に使用したホール素子 (AREPOC製、型番HHP-VP) の感磁面積は $50\mu\text{m}\times 50\mu\text{m}$ であり、素子の裏面にネオジム磁石を固定して、外部磁界 (ホール素子表面で 0.14T および 0.33T) を試料に印加した状態で測定を行った。測定間隔は x, y 方向共に 0.2mm とし、ホール素子と試料面との距離 (リフトオフ距離) は $0.5\text{--}3.5\text{mm}$ の範囲で変化させた。更に、鉄線での実験結果を踏まえた上で、 $60\mu\text{m}$ および $80\mu\text{m}$ 程度の平板状の鉄粉末を異物として塗布電極に混入させた場合についても測定を行った。

直径 $50\mu\text{m}$ 、長さ 1mm の鉄線を入れた LiCoO_2 塗布電極面上の二次元磁界分布の測定結果では鉄線の磁化による磁界分布が観測できた。リフトオフ距離 0.5mm および 2.5mm のいずれの場合においても、鉄線位置の近傍において鉄線の磁化に伴う磁界変化を検出できることが確認できた。また、リフトオフ距離の増加と共に検出磁界強度は大きく低下するが、金属近傍の磁界ピークの形状はブロードになっており、より広い範囲で鉄線の磁化による磁界変化が現れることが確認された。鉄線 (直径 $50\mu\text{m}$) の長さを変化させた場合、検出磁界のピーク値 $B_{z\text{-max}}$ は鉄線の長さにはほぼ比例して増減することが確認され、粒径 $50\mu\text{m}$ 程度の鉄粉末の有無を識別するためには、リフトオフを 1mm 以下にする必要があることが示唆された。また、測定感度向上に向けて、印加磁界 (ホール素子表面) を 0.14T から 0.33T に増加したところ、鉄線からの検出磁界強度がほぼ倍増することを確認した。

以上の結果を踏まえて、 $60\mu\text{m}$ および $80\mu\text{m}$ 程度の平板状の鉄粉末を混入した塗布電極表面の磁界分布を印加磁界 0.33T 、リフトオフ 0.5mm の条件で測定した。その結果、 $60\mu\text{m}$ の鉄粉末の場合、塗布電極自身が発生する磁界のため、鉄粉末の磁化による磁界変化は検出できなかったが、 $80\mu\text{m}$ の鉄粉末の場合、塗布電極の発生磁界に埋もれることなく鉄粉末の磁化による磁界変化を検出できた。今後、印加磁界方向とホール素子での検出磁界方向の組み合わせを調整することにより、更なる検出感度の向上を図ることが課題である。

Department of Electrical and Electronic Information Engineering		ID	071302	Supervisor	Ryoji Inada
Name	Abdul Azim Bin Jais				

Abstract

Title	Study for detection of metallic contaminant in electrode of lithium-ion battery using a Hall probe.
-------	---

Lithium-ion battery is commonly used for mobile power supply such as laptop and mobile telephone, because of its high energy density, but when malfunctions such as short circuit occurred inside battery, it could lead to ignition or explosion, and the battery safety is recognized as social problem. In process of battery production, metallic contaminant mix with parts of a battery can be a cause of short circuit inside battery. Therefore, it is necessary to detect at production stage. Study for detection metallic contaminant in battery using high temperature SQUID is currently in progress and by using this, 50 μ m ferromagnetic metal piece can be detected successfully. However, a cooling medium or cryogenic refrigerator is necessary for SQUID operation, so that the total measurement system becomes large size and expensive. On the other hand, Hall probe is known to be cheap and high versatility magnetic field sensor. Although measurement sensitivity of magnetic field for Hall probe is much lower than SQUID, by applying an external magnetic field can increase the field generated from magnetized metallic contaminant, resulting into increase for possibility to detect the metallic contaminant. In this research, we measured the magnetic field distribution of metallic contaminant in electrode for lithium-ion battery using Hall probe and examined the applicability for metallic contaminant detection technology that is more simple, easier and cheaper.

Electrode of lithium-ion battery (15mm \times 15mm, thickness 0.90mm) was made by coating cathode material, LiCoO₂ on Aluminum foil, and measurement sample were prepared by adding a piece of iron wire (diameter 50 μ m, length 0.5–2.0mm) on the electrode. The sample was put on a Bakelite sample holder, and a Hall-probe was placed on top of it and then was scanned two-dimensionally in x-y planar to examine distribution of magnetic field whose direction is perpendicular to sample surface (z-direction). Hall probe was made by AREPOC (HHP-VP) and its active area was 50 μ m \times 50 μ m. The field distribution of sample was measured under applied magnetic field by placing permanent neodymium magnet at the back of the probe. Applied external field that detected by probe were 0.14T and 0.33T. Measurement step for both x and y direction was 0.2mm, and probe lift-off distance from the sample surface was changed in 0.5–3.5mm. From the result of iron wire as a metallic contaminant, flat-shaped iron particle with diameter size of 60 μ m and 80 μ m was measured.

For electrode with iron wire with a diameter 50 μ m and a length 1mm, the field distribution of magnetized iron wire could be detected successfully. It was confirmed that the field from magnetized iron wire was detected at lift-off distance of both 0.5mm and 2.5mm. Also, when the lift-off distance was increased, detected field strength was decreased largely, while the peak width was appeared broad, and therefore, the field change caused by magnetized iron wire can be detected in wider range. In measurement for electrode with different length of iron wire but fixed diameter, maximum peak of detected field B_{Z-max} was increased proportionally to the length. From this result, the lift-off distance to detect iron particle with 50 μ m diameter was suggested to be set to 1mm and smaller. In order to enhance the measurement sensitivity, when applied field was increased from 0.14T to 0.33T, detected field strength from the sample with iron wire was increased double. Based on these results, to measure electrode with flat-shaped iron particle with diameter of 60 μ m and 80 μ m, measurement condition of 0.33T of applied field and 0.5mm of lift-off distance was determined. For iron particle with diameter of 60 μ m, the field from iron particle could not be detected because the field from iron particle was disturbed by that from the electrode. For iron particle with diameter of 80 μ m, the field from iron particle was detected due to not buried by field from the electrode. The direction of applied field and detected field by Hall probe should be adjusted for further improvement of measurement sensitivity as a task to be considered in future.

Study for detection of metallic contaminant in electrode of lithium-ion battery using a Hall probe

Table of Contents	Page
CHAPTER 1 Introduction	1
1.1 Research background and objective	1
1.2 Lithium-ion battery	2
1.2.1 Working principle of lithium-ion battery	2
1.2.2 Characteristic of lithium-ion battery	3
1.2.3 Application of lithium-ion battery	3
1.2.4 Problem of lithium-ion battery	4
1.2.5 Probability of metallic contaminant mix in lithium-ion battery at production stage	6
1.3 Metallic contaminant detection technology	7
1.3.1 X-ray inspection device	7
1.3.2 High temperature superconductor SQUID device	8
1.4 Hall probe	9
1.4.1 Introduction	9
1.4.2 Operation Principle of Hall probe	9
1.4.3 Characteristic of Hall probe	11
1.4.4 Precaution of using the Hall probe	12
1.4.5 Magnetic field distribution measurement device using Hall probe	12
1.4.6 Previous research by Hall probe and application for metallic contaminant detection	14
References	15
CHAPTER 2 Experimental Procedure	16
2.1 Introduction	16
2.2 Electrode for lithium-ion battery preparation procedure	16
2.2.1 Materials for electrode preparation	16
2.2.2 Electrode preparation	17
2.2.2.1 Material weight calculation method for LiCoO ₂ electrode preparation	17
2.2.2.2 LiCoO ₂ electrode preparation process	18

2.3	Measurement sample preparation method	21
2.3.1	Electrode with iron wire	21
2.3.2	Electrode with iron particle	22
2.4	Magnetic field distribution measurement	23
2.4.1	Applied magnetic field	23
2.4.1.1	Specifications of neodymium magnet	23
2.4.1.2	Magnetic field application method	24
2.4.2	Lift-off distance	25
2.4.3	Measurement step	25
	References	26

CHAPTER 3 Study on Magnetic Field Distribution of Electrode with Iron Wire

	Wire	27
3.1	Introduction	27
3.2	Magnetic field distribution of electrode with iron wire with different diameter	27
3.2.1	Iron wire with diameter 100 μm	28
3.2.2	Iron wire with diameter 70 μm	28
3.2.3	Iron wire with diameter 50 μm	28
3.2.4	Iron wire with diameter 20 μm	28
3.2.5	Iron wire diameter and lift-off distance dependence of magnetic field distribution	33
3.2.6	Discussion on magnetic field changed by lift-off distance	33
3.3	Magnetic field distribution of electrode with iron wire with different length	34
3.3.1	Iron wire with diameter 50 μm and length 2mm	34
3.3.2	Iron wire with diameter 50 μm and length 1mm	34
3.3.3	Iron wire with diameter 50 μm and length 0.5mm	34
3.3.4	The relation between iron wire length and magnetic field peak value	38
3.4	Discussion on magnetic field distribution measurement for electrode with iron particle	38

CHAPTER 4 Study for Enhancing Measurement Sensitivity of Magnetic Field Distribution	39
4.1 Introduction	39
4.2 Experimental procedure for enhancing magnetic field measurement sensitivity	40
4.3 Measurement Result	40
4.3.1 Applied magnetic field 0.14T	40
4.3.2 Applied magnetic field 0.33T	40
4.3.3 Discussion on the effect of increasing applied magnetic field	43
CHAPTER 5 Study on Magnetic Field Distribution of Electrode with Iron Particle	44
5.1 Introduction	44
5.2 Magnetic field distribution measurement of electrode with iron particle with different diameter	45
5.2.1 Iron particle with diameter of 80 μ m	45
5.2.1.1 SEM image	45
5.2.1.2 Magnetic field distribution	45
5.2.2 Iron particle with diameter of more than 100 μ m	47
5.2.2.1 Magnetic field distribution	47
5.2.3 Iron particle with diameter of 60 μ m	48
5.2.3.1 SEM image	48
5.2.3.2 Magnetic field distribution	49
5.3 Discussion about magnetic field generated from electrode	50
References	53
CHAPTER 6 Summary and Conclusion	54
Acknowledgements	56
Research achievement	57

CHAPTER 1 Introduction

1.1 Research background and objective

Recently, contaminant mixed in the industrial goods such as foods and electronic equipment has become a big social issue. Contaminant have two types which are metallic contaminant such as small piece of zinc, nickel, stainless steel, and non-metallic contaminant like stone, glass, plastic. When metallic contaminant mixed in foods, the danger that will occur to the consumers are like mouth cut, broken teeth and other health damage (physically injury), and then these make the consumer having unpleasant impression and lead to feel repulsion to the goods. When metallic contaminant mixed in electronic parts and equipment, it will cause trouble such as defective operation, breakdown and ignition. For the manufacturer, the problems are the reliability of product decreased, large-scale recall of goods and etc. therefore, social need of the detection of contaminant in industrial goods at the early stage is very high.

In this laboratory, as the research for lithium ion battery, the metallic contaminant mixed in battery parts at the production stage becomes a serious problem from the viewpoint of safety. Lithium ion battery is widely used for mobile power supply such as laptop and mobile telephone, and currently expanding into larger power supply for electric vehicle, hybrid car, energy storage and etc. As in high energy density, when malfunctions such as short circuit occurred inside battery, it could lead to ignition or explosion, and the battery safety is recognized as social problem. In process of battery production, metallic contaminant mix with parts of a battery can be a cause of short circuit inside battery. Therefore, it is necessary to detect at production stage. Currently, there is a detection device by X-ray or X-ray inspection could detect metallic and non-metallic contaminant. But, metallic contaminant of diameter $100\mu\text{m}$ and less could not be detected. While, study for detection metallic contaminant in battery using high temperature Superconducting QUantum Interference Device (SQUID) is in progress and by using this, $50\mu\text{m}$ ferromagnetic metal piece could be detected successfully⁽¹⁾. However, a cooling medium or cryogenic refrigerator is necessary for SQUID operation, so that the total measurement system becomes large size and expensive.

On the other hand, Hall probe is known to be cheap and high versatility magnetic field sensor. Although measurement sensitivity of magnetic field for Hall probe is much lower than SQUID, by applying an external magnetic field can increase the field generated from magnetized metallic contaminant, resulting into increase the possibility to detect the metallic contaminant.

In this research, we measured the magnetic field distribution of metallic contaminant in electrode for lithium-ion battery (coated electrode) using Hall probe and examined the applicability for metallic contaminant detection technology that is more simple, easier and cheaper.

1.2 Lithium-ion battery

1.2.1 Working principle of lithium-ion battery

Materials mainly used in lithium ion battery are lithium-containing transition metal oxide for positive electrode and graphitized-carbon material for negative electrode. The charge and discharge reaction of lithium ion battery is based on simple reaction of lithium ion move between the active material of positive and negative electrode through the electrolyte⁽²⁾. The working principle of lithium ion battery is, first of all, in the charge state of battery, lithium ion stored in positive electrode is detached and moved through the electrolyte and inserted between the interlayer of negative electrode (graphite electrode). By this movement of lithium ion and electron, lithium ion battery is charging. In the discharge state of battery, the movement of lithium ion and electron is reversed, which lithium ion stored in negative electrode is moved through the electrolyte and inserted into the positive electrode. Figure 1.1 illustrates the working principle of lithium ion battery (in the discharge state).

The best characteristic of lithium ion battery compared to Nickel-Metal Hydride (NiMH) battery, Nickel-Cadmium (NiCd) battery, lead acid battery and other secondary batteries or rechargeable batteries is high voltage, which about 4V. Therefore, water which has theoretical decomposition voltage 1.23V cannot be used as electrolyte, but non-aqueous electrolyte has to be used by dissolving electrolyte salt in organic solvent.

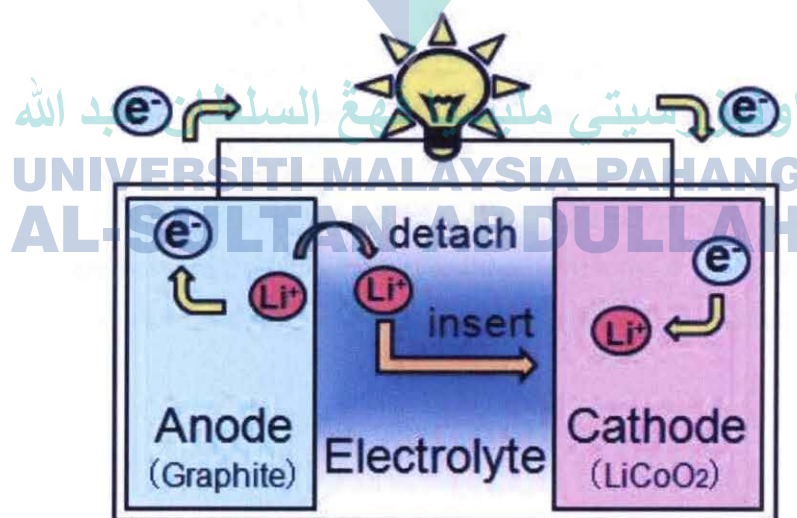


Figure 1.1 The working principle of lithium-ion battery (in the discharge state)

1.2.2 Characteristic of lithium-ion battery

Batteries have become useful in our general daily life and are put to even greater use of it in wider field in the future. Batteries are divided into two categories, primary batteries that have to disposal after used and secondary batteries that can be used again by charging. The later is in the charge state when electrical energy is applied and lead to chemical reaction. Thus, the secondary battery is a conversion and storage device of electrical energy into chemical energy. The secondary battery such as lithium ion battery, which is useful for mobile phone, laptop, car and etc., and as an efficient rechargeable battery, its existent is absolutely necessary for the society. Lithium ion battery, from the history of battery development, it has been used since 1991 and has characteristic such as small size, light weight, high open circuit voltage, and high energy density, etc. There are still continually having the demands for lithium ion battery even had been used about 20 years ago, and recently, not only in our daily life but also in other different kinds of field at sea, sky, space and many more is spread widely.

1.2.3 Application of lithium-ion battery

The production of Lithium ion battery was started by SONY in 1991⁽²⁾. At first, it was installed in video camera because of its merits which are small self-discharge and large energy density. After that, because of the introduction of battery for mobile phone (100% lithium ion battery currently installed) and laptop, its market has been expanded every year. At present, the application has expanded to electrical power tool, portable music device, game console and so on⁽⁴⁾. Especially lithium ion battery for car is being expected. In recent years, the influences of greenhouse effect caused by increasing exhausted carbon dioxide and sudden increased of oil and gas price had come to the surface globally, therefore in the industrial of car, hybrid vehicles, plug-in hybrid vehicles, and electric vehicles are being introduced to tackle these problems. In the present state, lithium ion battery for car has been started being sold and the demands will be expected to increase in the future.

1.2.4 Problem of lithium ion battery

The problem of lithium ion battery is there are market troubles of battery related to safety and battery recall since had been used in year 1995 until year 2007. Table 1.1 shows the recall of lithium ion battery.

From Table 1.1, the reason for recall of battery cases is more to internal short circuit⁽⁵⁾. Furthermore, other reason is exothermic phenomenon. When lithium ion battery is exposed to high temperature such as dropped into the fire, chemical reaction in lithium ion battery is rapidly occurred, these could resulted to start smokes, ignition, and explosion, and other hazardous situation. In addition, the contaminant mixed in during the production stage of battery or metal deposits inside battery can cause the internal short circuit and other occurred, as the reason of this, the temperature of battery is increased and the battery is chain reaction self-heated. In case of the heat dissipation is not enough, the smoke, the ignition, and other hazardous situation would be happened. The other reasons that generate self-heating of battery are thermal decomposition of electrolyte, reaction between cathode and electrolyte, and reaction between lithium insertion anode and electrolyte, etc.⁽⁵⁾.

Table 1.1 The recall of lithium ion battery⁽⁵⁾⁽⁶⁾⁽⁷⁾

Year	Battery-used device	Trouble outline	Probable cause
1995	Note PC	Ignition	Abnormal charge
1996	Mobile phone	Explosion	Crush (internal short circuit)
1997	Note PC	Combustion	Internal short circuit (?)
1998	Note PC	Generation of heat	Short circuit by liquid leakage
1999	Note PC	Bag case melt	Internal short circuit (?)
1999	Video camera	Generation of heat	Short circuit by liquid leakage?
1999	Mobile Phone	Generation of heat and explosion	Internal short circuit
2000	Video Camera	Generation of heat and smoke	Short circuit by liquid leakage?
2000	Note PC	Ignition	Internal short circuit?
2000	Note PC	Generation of heat and smoke	Abnormal protection circuit?
2000	Mobile Phone	Swelled and could not be used	Poor weld?
2001	Mobile Phone	Generation of heat	Solder joint failure
2002	Mobile Phone	Ignition	Production failure?
2003	Mobile Phone	Generation of heat	Circuit fault?
2003	Mobile Phone	Explosion	Internal short circuit (non genuine product)

2004	PC	Ignition	Internal short circuit
2004	Fishing reel	Ignition	Internal short circuit
2005	Digital audio	Generation of heat	Internal short circuit
2005	Digital camera	Generation of heat	Internal short circuit
2005	DVD player	Generation of heat	Internal short circuit
2005	Mobile Phone (America)	Explosion	Internal short circuit?
2006	Mobile Phone	Battery pack swelled	Overcharged
2006	PC	Generation of heat and ignition	Internal short circuit
2006	PC	Generation of heat by fall	Battery pack production failure
2006	Scooter etc	Generation of heat and ignition	Internal short circuit
2006	Mobile Phone	Generation of heat and explosion	Internal short circuit
2007	PHS, Mobile Phone	Generation of heat by impact	Internal short circuit
2007	PC	Generation of heat and ignition	Internal short circuit
2007	Mobile Phone	Ignition and explosion	Internal short circuit
2008	Mobile Phone	Generation of smoke and ignition	Internal short circuit by external collision
2008	Digital audio	Ignition	Internal battery damaged by defective parts
2009	Note PC	Ignition and fire	Mixed with contaminant
2009	Portable TV	Generation of smoke and ignition	Under investigation
2011	Mobile Phone	Generation of heat	Internal short circuit

1.2.5 Probability of metallic contaminant mix in lithium ion battery at production stage

Figure 1.2 shows the standard production process of lithium ion battery. First of all, the slurry of electrode active materials mixture is made to make coating electrode (cathode and anode) of lithium ion battery. Then, electrode current collector is coated by the slurry using a coater, and winded up after dried. The thickness and width of the electrode is adjusted by roller press and cut using slitter. Here, there is a possibility that a small piece of iron and other metal from the slitter mix in the electrode. Furthermore, a group of electrode is put into battery tube after winded, then the terminal is put on and finally the battery is completed. There is a case that inside wall of the battery tube is coated by thin layer of nickel, and therefore there is a possibility that a small piece of nickel peel-off during swaging process and mix in the battery parts.

Metallic contaminant that mixes in lithium ion battery not only causing the battery longevity decreased, but also there is possibility to generate heat and the worst case is to cause the ignition. As its application for hybrid vehicle and electrical car would be introduced, the important to prevent metallic contaminant from mix into battery part is increased, and thus for this matter the prevention of metallic contaminant mix in during the production process of lithium ion battery is essential. In addition, the detection of metallic contaminant mix in the material, and the development of technology to detect at the early stage of production process are also important.

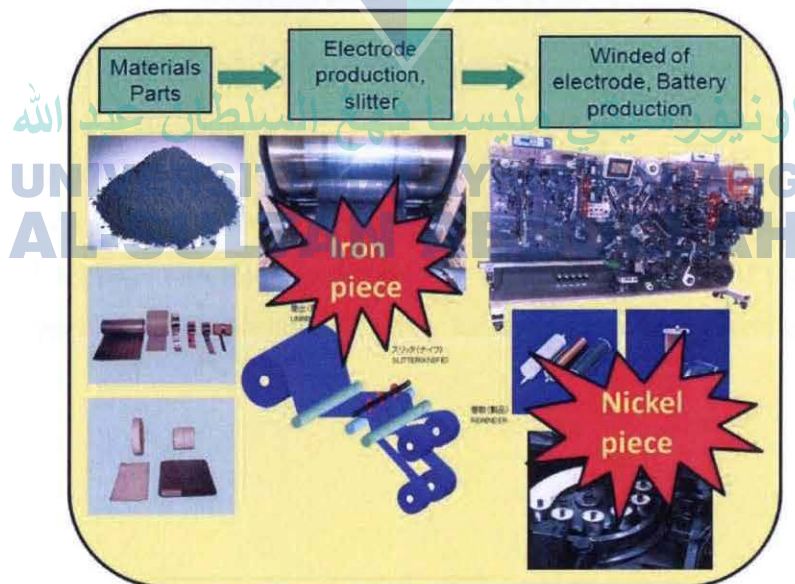


Figure 1.2 The possibility of metallic contaminant mix in during production stage of Lithium-ion battery

1.3 Metallic contaminant detection technology

1.3.1 X-ray inspection device

X-ray inspection device is configured with X-ray radiation tube that can generate soft X-ray, line sensor that can measure X-ray transmission amount and etc. X-ray that generated from radiation tube is transmitted through inspection goods and then the transmission rate is measured by line sensor. When there is no inspection goods, because of X-ray is transmitted 100%, transmission rate become 100%. But when there is inspection goods, transmission rate is decreased due to X-ray was absorbed. In case of contaminant was mixed in the inspection goods, the transmission rate that lower than the normal one from the goods is recognized as signal from contaminant.

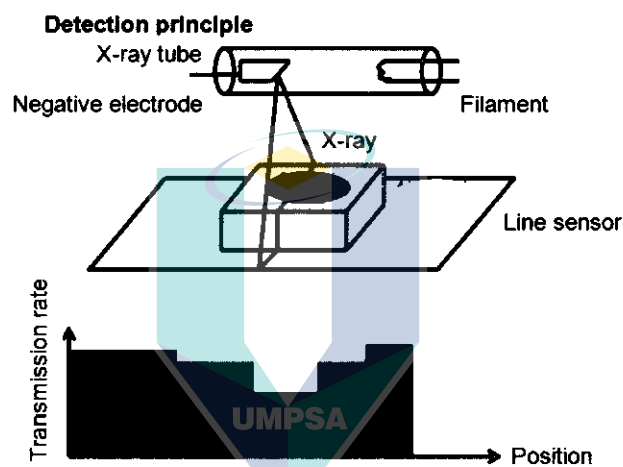


Figure 1.3 Principle of X-ray inspection device

At the present, X-ray inspection device could detect metallic contaminant with size more than $100\mu\text{m}^{(8)}$. Also, could detect plastic, bones and other non-metallic contaminant.

However, the disadvantage of X-ray inspection device is difficult to detect things with small specific weight such as hair, rust and etc. Moreover, there is a problem of the viewpoint of safety such as X-ray leakage, and it is important to strictly handle and safety control the device.

1.3.2 High temperature superconductor SQUID detection device

SQUID is derived from Superconducting Quantum Interference Device. The quantized magnetic field is formed in the hole of superconductor ring as magnetic flux. This phenomenon was used by superconducting electron probe known as SQUID that could be used as high sensitivity magnetic sensor.

The detection technology of metallic contaminant using high temperature superconductor SQUID is recently developed⁽¹⁾, and the outline diagram is shown in Figure 1.5. Figure 1.4 shows the shape of high temperature superconductor SQUID sensor used in the device.

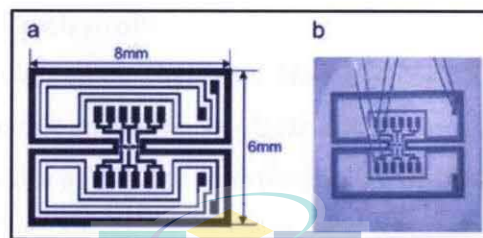


Figure 1.4 High temperature superconductor SQUID sensor

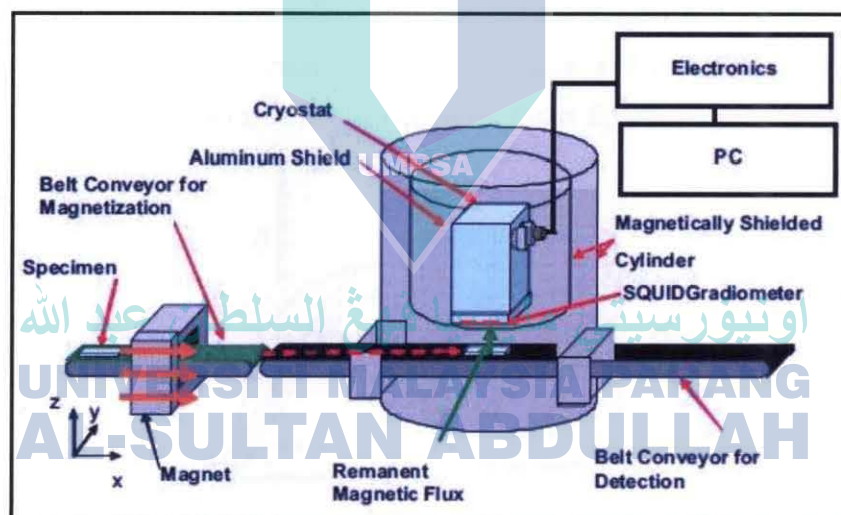


Figure 1.5 Outline diagram of the detection technology of metallic contaminant using high temperature superconductor SQUID .

Using this device, after the sample is magnetized, high temperature superconductor SQUID sensor is measuring the remanent magnetic field of sample and detecting remanent magnetic field of metal piece, this device can be used at production line to detect a very small piece of metallic contaminant. The measurement sensitivity of SQUID is high that about 50 μ m ferromagnetic metal piece can be detected was reported.

However, a cooling medium or cryogenic refrigerator is necessary for SQUID operation, therefore this would lead to the problem such as total measurement system becomes large size and expensive.

1.4 Hall probe

1.4.1 Introduction

Hall probe that used for the magnetic field measurement is two-dimensionally scanned on sample surface. Thus, two-dimensional magnetic field distribution of sample could be measured. First, Hall probe, which can measure magnetic field, and the composition of magnetic field measurement device that using it are explained in details below. And, the example of previous research that used Hall probe is also described.

1.4.2 Operation principle of Hall probe

Hall probe is a magnetic field sensor that used Hall Effect, or known as Hall Effect magnetic sensor, which can directly change magnetic to electric. Figure 1.6 shows a rectangular section of thin conductor (thickness t , width a) is placed vertically in a uniform magnetic field (magnetic flux density B), and the current I is considered to flow in x direction. Then, the current flow in the conductor is carried by electron that is moved in $-x$ direction. The electron moved with velocity v is resulted to Lorentz force $F = ev \times B$ due to the existence of magnetic flux density, that cause the electron is collected at $-y$ direction of conductor edge and positive charge at y direction of conductor edge. These then generate the electric field $E_y = E_H (< 0)$.

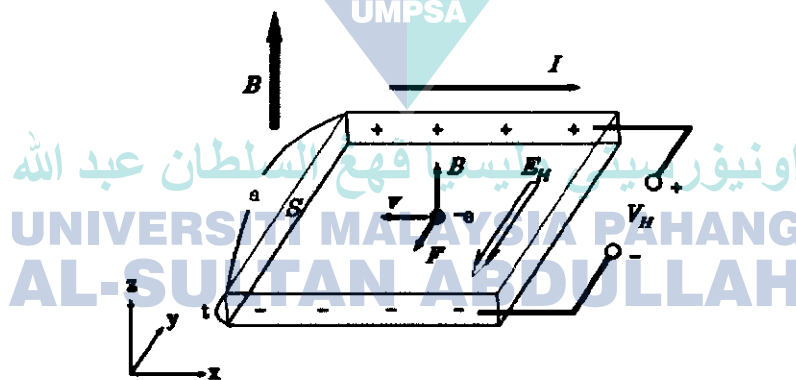


Figure 1.6 Hall Effect

In the stationary state, the point of electron is considered to move only in x direction, not in y direction to find the value of E_H . The balance of force by electric field E_H and force by magnetic flux density is assumed to become

$$E_H = vB \quad (1 - 1)$$

Using the relation between velocity of electron and density of current, $i = -nev$

$$I = iS = -nevS \quad (1 - 2)$$

is obtained.

Here, $S = at$ is sectional area of conductor plate. Then, it becomes

$$E_H = \frac{IB}{neS} \quad (1 - 3)$$

Electric potential, generated by Hall Effect in y direction becomes

$$V_H = -E_H a = \frac{IB}{net} = R_H \frac{IB}{t} > 0 \quad (1 - 4)$$

This is known as a Hall voltage. If the current that assumed as charged particles is positive, it become $E_H > 0$ and $V_H < 0$ with sign inversion. Here, B is the external field of magnetic flux and $|R_H| = 1/ne$ can be written where R_H is the Hall coefficient, e is electron charge, and n is carrier density. From equation(1 - 4) , to obtain large V_H , thin layer of active material, material with small carrier density and large amount of current is necessary.

At the present, material of Hall probe is mainly semiconductor with III-V family compound such as GaAs, InSb, Si and other. Hall coefficient is influenced by electron mobility, thus semiconductor with high mobility tend to be the material as listed above. The structure of Hall probe is formed with 2 output electrodes, and active layer. The active layer is formed by deposition of InSb, injection of ion in GaAs and other appropriate method of each material. As a result, output voltage of Hall probe is actually smaller than that calculated from equation (1 - 4) as electrode shape is assumed as a point, in constant current operation, V_H is

$$V_H = G_H R_H \frac{IB}{t} \quad (1 - 5)$$

and in constant voltage operation,

$$V_H = G_H \frac{w}{l} \mu \times V \times B \quad (1 - 6)$$

can be expressed where μ is hole mobility, G_H is pattern factor, w and l is pattern width and length respectively. For lead frame, non-magnetic material must be used.

1.4.3 Characteristic of Hall probe

The output characteristic of an ideal Hall probe is assured to be shown according to equation (1 – 5) and (1 – 6), but is actually depend on the non-uniformity of current distribution during crystallization, atmosphere temperature and the magneto-resistance effect.

(1) Unbalanced voltage

For an ideal Hall probe, when $B = 0$, equation (1 – 4) should become $V_H = 0$, but in fact, because of the non-uniformity of current distribution during crystallization and asymmetric main terminal, even without the presence of external magnetic field, the voltage is slightly generated. This is known as unbalanced voltage. Furthermore, it is important to care that the balanced voltage is depending on atmosphere temperature.

(2) Temperature dependence

The output voltage of Hall probe is decreased with the increasing atmosphere temperature. This phenomenon is occurred in both case of constant voltage operation and constant current operation. From equation(1 – 6), at constant voltage operation, it contributed from hole mobility temperature dependence is known. As well as equation(1 – 5), temperature dependence of constant current operation is influenced by carrier mobility temperature dependence is also known. Therefore, the temperature dependence of output voltage should be as small as possible, in case either at constant voltage or constant current operation, the material of Hall probe should be selected with magnitude relation to temperature dependence of carrier density and hole mobility.

(3) Magnetic field dependence

Equation (1 – 6) shows the proportional relation between Hall voltage and external magnetic field. However, in fact, the tendency of saturation is shown due to the external magnetic field. This is called the magneto-resistance effect. The magneto-resistance is the phenomenon where the resistance in Hall probe is increased when its current path become longer due to Hall probe driving current path bended caused by the Lorentz Force due to the existence of external magnetic field. According to this, the voltage applied between input electrodes is becoming small compared to the actual value, and the geometrical factor in equation(1 – 6) is magnetic field dependence, decreased with increasing external magnetic field. This shows overall is magnetic field dependence. Therefore, to obtain probe with good linearity due to existence of external magnetic field, material that has small magneto-resistance effect and pattern with small geometrical factor have to be chosen.

1.4.4 Precaution for using Hall probe

When using Hall probe for the measurement, it is important to use carefully and correctly according to its characteristic. There is a problem which to consider either constant current or constant voltage operation has to be used. In term of Hall voltage accuracy, constant current operation should be used. The reason is because when constant voltage operation is used, due to magneto-resistance, the Hall probe length value l in equation(1 – 6) is becoming large and this could be significant effect to the Hall voltage. On the other hand, in case of using constant current operation, as shown in equation(1 – 5), Hall voltage with no distortion could be obtained because does not influenced by probe length value l .

However, at the operation of constant current, although current is constantly flew through Hall probe, if the resistance of Hall probe is changed by magneto-resistance effect, voltage value that applied to Hall probe could be changed. This can be resulted to the temperature change in unbalanced voltage that leads to its temperature characteristic decreased and therefore need to take attention.

1.4.5 Magnetic field distribution measurement device using Hall probe

Figure 1.7 illustrates the magnetic field distribution measurement device using Hall probe. Hall probe is fixed at the end of Bakelite arm and is attached to x - y stage of device. From this, Hall probe is moved in two-dimension on the surface of sample. Constant current of 10mA was used to drive Hall probe. Measurement result is obtained by reading voltage value of digital voltmeter and calculating magnetic flux density by the calibration with Hall coefficient. In addition, when applying current to the Hall probe for magnetic field distribution measurement, direct current supply is used and its amount can be controlled by PC. The image of Hall probe for measurement is shown in Figure 1.8 and its specifications are shown in Table 1.2. As shown in Figure 1.8, Hall probe is located at the centre (sign of +) of the package, and 0.5mm of distance from package surface. This corresponds to the minimum lift-off distance of Hall probe from the sample. However, in fact, lift-off distance might be increased due to use of tape for setting up the sample. Moreover, magnetic field component that detected by Hall probe is in the normal direction (z) against package plane (and sample plane).

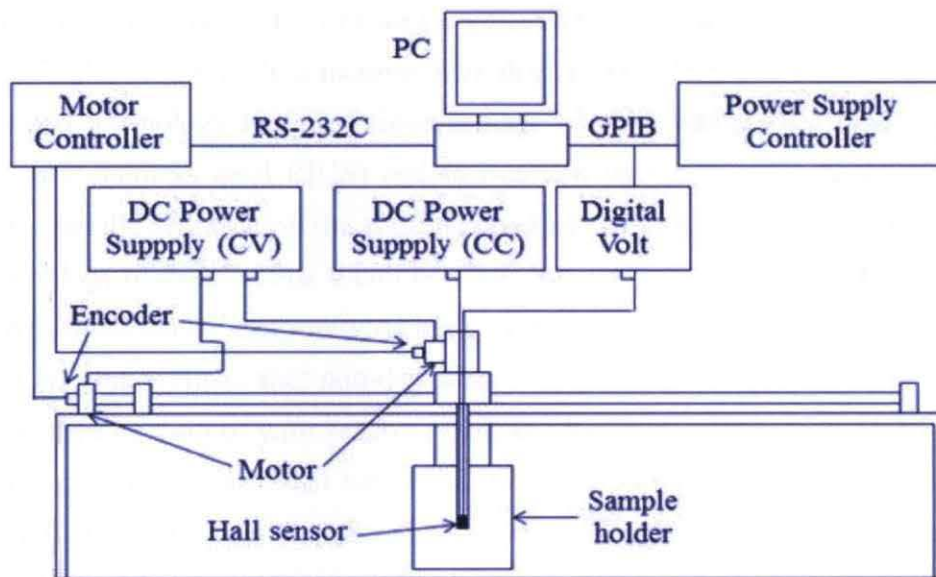


Figure 1.7 Illustration of magnetic field distribution measurement device using Hall probe

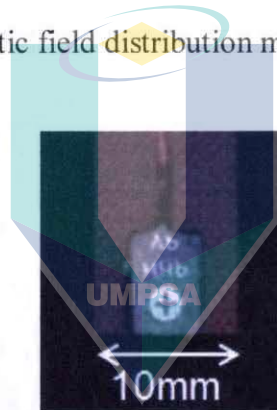


Figure 1.8 Image of Hall probe (view of package plane)

Table 1.2 Specifications of Hall probe

Manufactured by AREPOC	
Model number	HHP-VP
External dimension	7 × 5 × 1 [mm]
Sensitivity	78.3 [μV/T]
Lift-off distance	0.5 [mm]
Active area	50 × 50 [μm]

1.4.6 Previous research by Hall probe and application for metallic contaminant detection

In the research, the magnetic field measurement device using Hall probe, at first, the application of instrumentation technology to find fatigue damage of steel was studied, and micro-crack and fatigue growth on stainless steel (SUS) and low-carbon steel rod could be evaluated has been confirmed. The specific research on the welding point of SUS pipe and the application for quality evaluation technology of Friction Stir Welding (FSW) material on SUS-A1 has been also examined. In addition, the evaluation of uniformity of high temperature superconductor by using this device was successfully done. Also, the non-destructive evaluation of non-uniformity of electrical characteristic in the direction of wire section width and longitudinal direction of Ag-sheathed high temperature superconducting wire that has been introduced with high resistivity barrier and twisted superconductor filament in order to reduce A_c losses had been carried out successfully using the device⁽¹⁰⁾⁽¹¹⁾.

On the other hand, magnetic field detection sensitivity is the most important in order to use magnetic sensor for detection of metallic contaminant mixed in battery parts. The detection sensitivity of Hall probe is shown in Figure 1.9, and its fundamental weak point is low in several digits compared with SQUID. However, if metallic contaminant is limited to iron and other ferromagnetic metal, and by applying external magnetic field, the magnetized contaminant will increase generating magnetic field that can be detected. Thus, the weak point can be countered and there is a possibility to the application of metallic contaminant detection technology is suggested.

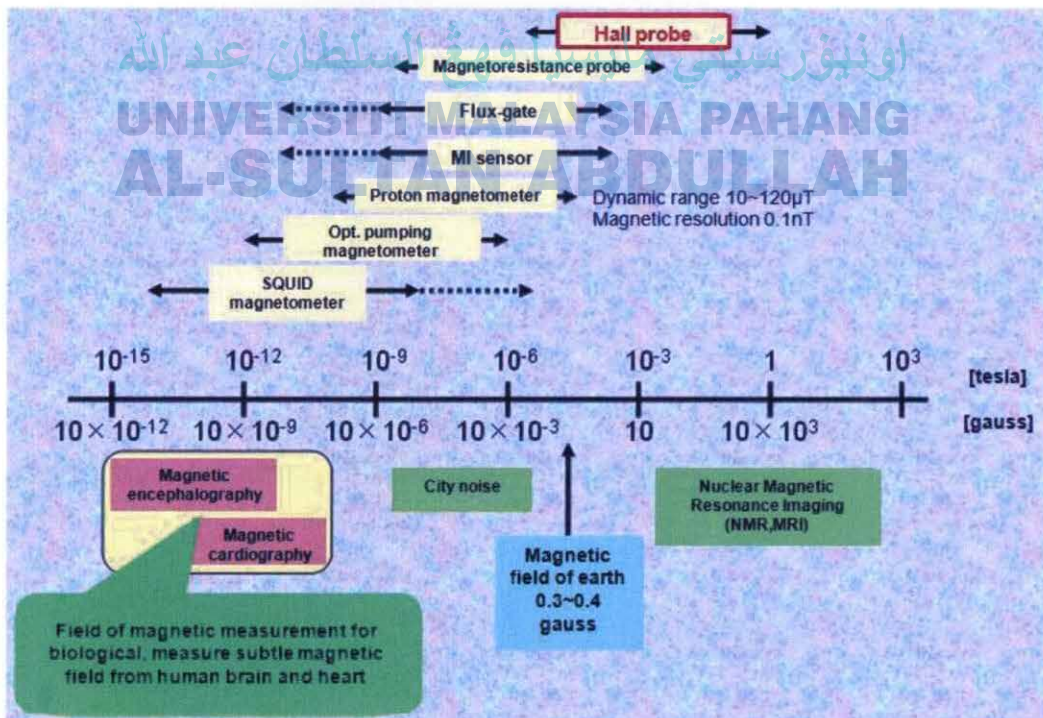


Figure 1.9 Types of magnetic sensor and detection sensitivity

References

- (1) S. Tanaka, et al. : J. Magn. Magn. Mater. 324(21), pp. 3487-3490. (2012)
- (2) 小澤秀清 : 「最新リチウムイオン二次電池「～安全性向上および高機能化に向けた材料開発～」」、情報機構 (Chapter 2, Section 2, Paragraph 1) (2008)
- (3) 日経エレクトロニクス、日経ものづくり、日経 Automotive Technology、日経エコロジー編 : 「次世代電池 2007/2008」、日経 BP 社 (2007)
- (4) 吉野彰監修 : 「リチウムイオン電池この 15 年と未来技術」、シーエムシー出版 (2008)
- (5) 鳶島真一 : 「最新リチウムイオン二次電池 ～安全性向上および高機能化に向けた材料開発～」」、情報機構 (Chapter 1, Section 1) (2008)
- (6) <http://bizmakoto.jp/makoto/kw/ignition.html>
- (7) <http://www.nite.go.jp/index.html>
- (8) 軟 X 線異物検出機の原理と留意点(Principle and precautions of soft X-ray inspection device):
https://sv49.wadax.ne.jp/~food-eng-jp/?action_user_view=1&r=KyrHwVxnWil109
- (9) http://www.anritsu-industry.com/ja-JP/products/contaminant/pdf/Xray_h_43543_E_1.pdf
- (10) 馬場翔平 : 豊橋技術科学大学修士学位論文 (2009)
Master thesis, Toyohashi University of Technology, (2009)
- (11) 荒木優次 : 豊橋技術科学大学修士学位論文 (2008)
Master thesis, Toyohashi University of Technology, (2008)
- (12) A. Oota, et al. : Rev. Sci. Instrum. Vol. 70, 184-186. (1999)
- (13) 篠原義和 : 豊橋技術科学大学修士学位論文 (2011)
Master thesis, Toyohashi University of Technology, (2011)
- (14) High temperature superconductor SQUID :
<http://www.istec.or.jp/web21/series/2001-itozaki.pdf>
- (15) 食品製造現場における金属異物混入防止の考え方と進め方(Ideas and methods for prevention of metallic contaminant at foods manufacturing site) :
<http://www.ikari.co.jp/topics/professional9.html>
- (16) Hall probe : http://www.riam.kyushu-u.ac.jp/gikan/report/06/hall_element.pdf
- (17) <http://www.kbrasch.co.jp/solution/dr.escherich/lithiumionbattery/>
- (18) 【Sakurai and Inada Laboratory】Laboratory Introduction slide 2012

CHAPTER 2

Experimental Procedure

2.1 Introduction

First of all, we explain the method for the preparation of the electrode of lithium ion battery in this chapter. In our research, lithium cobalt oxide, LiCoO₂ (Nippon Chemistry Industrial Co., Ltd.) was used as cathode material to prepare the electrode coating⁽¹⁾. After that, measurement sample was made by adding a piece of metallic contaminant in the prepared electrode. The preparation of measurement sample, the method of measurement, the method of analysis and evaluation were explained here. Iron wire and iron particle were used for metallic contaminant in our research as well.

2.2 Electrode for lithium-ion battery preparation procedure

2.2.1 Materials for electrode preparation

In our research, lithium cobalt oxide (LiCoO₂), now widely used as positive electrode or cathode for lithium ion battery, was used to prepare the electrode. Also, acetylene black (AB) was used as conducting material. The specifications of LiCoO₂ and AB as materials for the preparation of the electrode are showed in table 2.1 and 2.2. Moreover, PolyVinylidene diFluoride (PVdF) was used as the electrode binder material for cathode and N-methyl-2-pyrrolidone (NMP) was used as a solvent, and the specifications of both materials are showed in table 2.3 and 2.4 respectively.

Table 2.1 The specifications of LiCoO₂

Name or Label	C-10
Manufacturer	Nippon Chemical Industrial Co., Ltd.
Average particles size (μm)	10.5
Specific surface area (m ² /g)	0.21

Table 2.2 The specifications of AB

Name or Label	Acetylene Black
Manufacturer	Nippon Chemical Industrial Co., Ltd.
	50 % press

Table 2.3 The specifications of PVdF

	Binder material for cathode
Name or Label	L#7208
Manufacturer	Kureha Corporation
The resin content (%)	8
Weight average molecular weight	About 630 thousand
Thickness (mPa·s)	2350
Moisture (%)	≤ 0.1

Table 2.4 The specifications of NMP

Name or Label	N-methyl-2-pyrrolidone
Manufacturer	Kishida Chemical Co., Ltd.
Purity (%)	99.5
Chemical formula	CH ₃ NC ₄ H ₆ O

2.2.2 Electrode preparation

2.2.2.1 Material weight calculation method for LiCoO₂ electrode preparation

LiCoO₂ cathode was made by based on the weight ratio, LiCoO₂:AB:PVdF:NMP = 90:6:4:90, that the cathode slurry was made and coated on aluminum foil. The material weight calculation is showed as below.

1. Weight of LiCoO₂

LiCoO₂ was assumed to be 7 g.

2. Weight of AB

Weight of AB is written as M_{AB}g and calculated as shown below

$$90:7 = 6:M_{AB}$$

$$M_{AB} = \frac{6 \times 7}{90} = \frac{42}{90} \approx 0.4667 \text{ g}$$

3. Weight of PVdF

Necessary Weight of PVdF solid component in the binder solution is written as M_{PVdF} , and calculated same like AB.

$$90:7 = 4:M_{PVdF}$$

$$M_{PVdF} = \frac{7 \times 4}{90} = \frac{28}{90} \approx 0.3112 \text{ g}$$

Solid component of PVdF solution is 8wt.%, therefore necessary weight of PVdF solution is written as $M_{PVdF_sol'n}$ g and become

$$1:0.08 = M_{PVdF_sol'n} : 0.3112 \text{ g}$$

$$M_{PVdF_sol'n} = \frac{0.3112}{0.08} = 3.89 \text{ g}$$

4. Weight of NMP

Weight of NMP in PVdF solution as a solvent is

$$3.89 \text{ g} - 0.3112 \text{ g} = 3.5788 \text{ g}$$

Weight of NMP needed is written as M_{NMP} and calculated as shown below.

$$90:7 = 90:M_{NMP}$$

$$M_{NMP} = \frac{90 \times 7}{90} = 7 \text{ g}$$

Thus, necessary weight of NMP to be used is

$$7 \text{ g} - 3.5788 \text{ g} = 3.4212 \text{ g}$$

2.2.2.2 LiCoO₂ electrode preparation process

LiCoO₂ electrode preparation process is showed in Figure 2.1. The details of the procedure are described in the following 1-10.

1. LiCoO₂ and AB were used and weighed respectively based on the weight ratio, LiCoO₂:AB=90:6, that was calculated by electron balance, and was put in pot 2 (Kinki Container, BHR-150, 150cc). The total weight of the sample in pot 2, pot 2 and mixer adaptor were weighed and the sample was mixed using the planetary mixer at 2000 rpm in 5 min.
2. PVdF and NMP solution were used and weighed respectively based on the weight ratio, PVdF:NMP =4:90, that calculated by electron balance, and was put in pot 1. The total weight of the sample in pot 1, pot 1 and mixer adaptor were weighed and the sample were mixed using the mixer at 1000rpm in 1 min.

3. The sample mixture in pot 2 was weighed and calculated by electron balance after the mix procedure, and put in pot 1. The total weight of the sample mixture in pot 1, pot 1 and mixer adaptor were weighed and the mixture were mixed again using the mixer at 2000 rpm in 5 min for mixing and then at 2200 rpm in 30 sec for defoaming, and repeated for 3 sets. The slurry of cathode mixture was obtained.
4. Aluminum foil (Thank-Metal Co. Ltd., Al 0.020 mm) was set on the coater in the clean booth. Then, the height of the applicator was set to 10 mil as to make the thickness of coating is constant. After the Aluminum foil was wiped with the acetone and the coater memory was set to 100, the cathode slurry was coated on the Aluminum foil.
5. After coating procedure, the first drying process was done using far infrared radiation (Quick Ultra Thermostat QUT60BTL) at 110 °C in the clean booth.
6. After the first drying process finished, the second drying process of the electrode was done using vacuum dryer at 120 °C in 12h.
7. After the second drying process finished, the electrode was taken out and cut into 15mm × 15mm size of square.
8. Then, the electrode was press 2 times using Newton Press Equipment at 21 kN (93.3 MPa).
9. After that, the electrode was dried naturally in vacuum dryer at 80 °C for 12h.
10. When the process finished, the LiCoO₂ cathode was prepared.

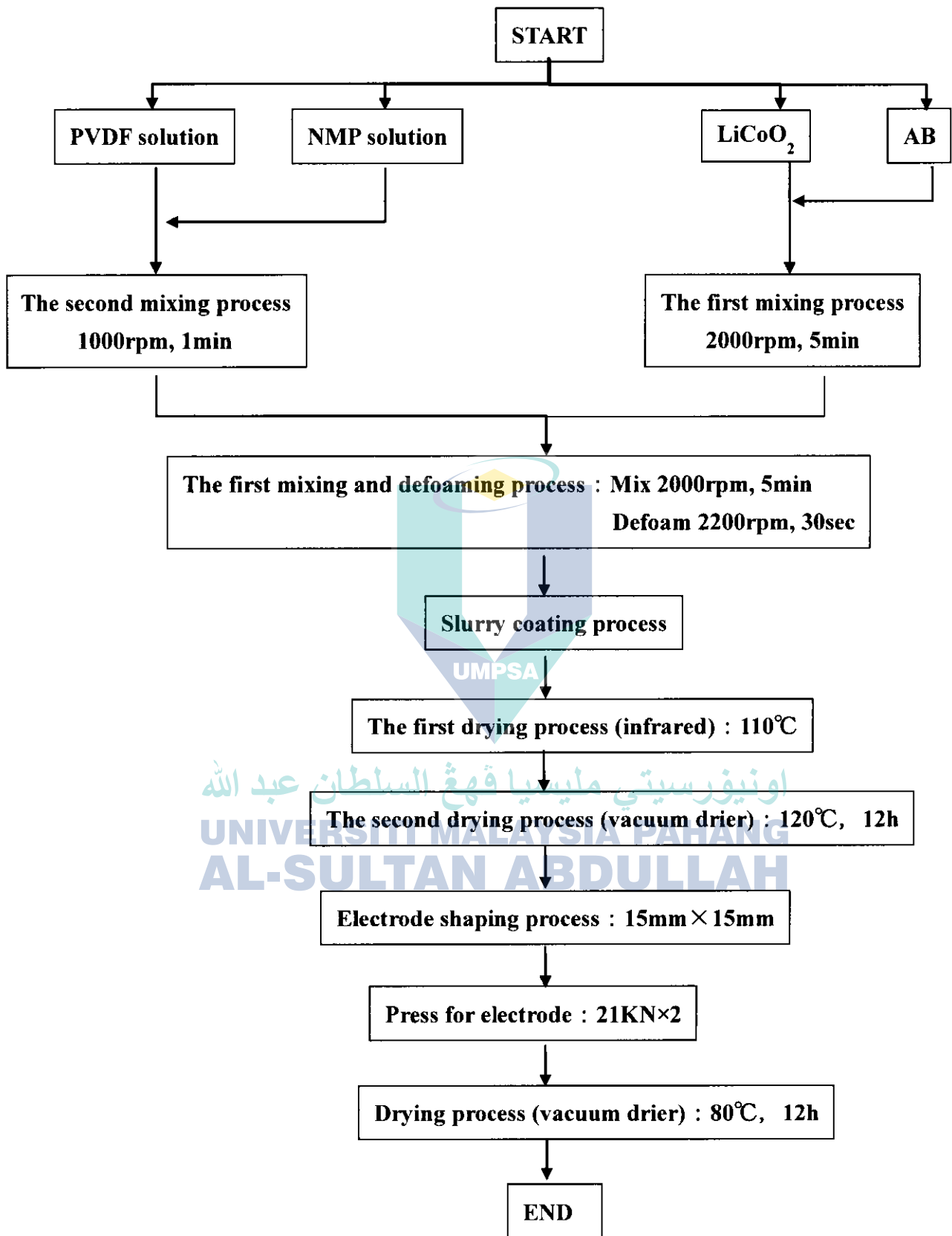


Figure 2.1 Lithium cobalt oxide electrode preparation process

2.3 Measurement sample preparation method

2.3.1 Electrode with iron wire

In this research, the measurement sample was made by adding a small piece of iron wire (Omega Engineering co., ltd.) as metallic contaminant in the prepared cathode. First, 100,70,50,20 μ m of different diameter size of iron wire were used and cut into 1mm length respectively to confirm the diameter of wire dependency of the magnetic field distribution. The prepared iron wire is showed in Figure 2.2. Moreover, to evaluate the effect of the change in length of iron wire on the magnetic field distribution, iron wire with 50 μ m diameter was used and cut into different length of 0.5,1,2mm. The relation between the study content and the iron wire used is summarized in Table 2.5 respectively.

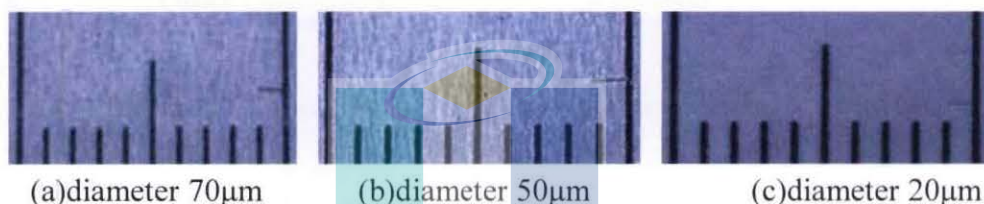


Figure 2.2 Iron wire with diameter of 70,50,20 μ m and length of 1mm

Table 2.5 The measurement sample parameter of each study

Study	Diameter of iron wire (mm)	Length of iron wire (mm)
Diameter of wire dependence of magnetic field distribution	100	1.0
	70	
	50	
	20	
Magnetic field distribution by the change in wire length	50	0.5
		1.0
		2.0

The magnetic field distribution measurement was done using a Hall probe after the prepared electrode was mixed with a small piece of iron wire and set up on sample holder. Details of the procedure are shown in the following 1-3.

1. The small piece of iron wire was set up on Bakelite material sample holder using kapton tape.
2. After that, the electrode was put on top of it and fixed using kapton tape.
3. The magnetic field distribution measurement on the electrode was done using a Hall probe.

2.3.2 Electrode with iron particle

Instead of iron wire, iron particle was used as metallic contaminant. Table 2.6 shows the specifications of the iron particle.

An iron particle with diameter of 60, 80 and more than 100 was picked up respectively and mixed into the electrode, and then the detection of contaminant in the electrode was studied.

Table 2.6 The specifications of iron particle

Name or Label	Fe Powder
Manufacturer	Kojundo Chemical Laboratory co., ltd.
Average diameter (μm)	53
Purity	99%up

Details of the procedure to pick up the iron particle and the evaluation method of it are shown below.

1. A small amount of iron particle was mixed into dehydrated ethanol and ultrasonic dispersion was done for 30 min. A transparent polypropylene (PP) film was hold on to slide glass and several drops of ethanol containing iron particle was dropped on it and dried naturally.



Figure 2.3 Dropped of iron particle

2. While the iron particle was observed by stereomicroscope, one predetermined size of iron particle was picked up using iron wire (diameter of 50 and 20), and then moved on to carbon tape for SEM observation. Furthermore, for measuring the magnetic field distribution, the similar iron particle was picked up and moved on to the kapton tape.
3. The iron particle that was picked up earlier was hold on the Bakelite material sample holder using kapton tape and the magnetic field distribution was measured using a Hall probe.
4. After the measurement finished, the electrode was put on top of iron particle and set up on the sample holder properly. Then, the magnetic field distribution was measured again using a Hall probe.

2.4 Magnetic field distribution measurement

After the measurement sample had been setting up on the sample holder, the magnetic field distribution measurement was done using a Hall probe with the measurement condition had been set. Set-up procedure of the magnetic field distribution measurement and details of the measurement condition are described as follows.

2.4.1 Applied magnetic field

2.4.1.1 Specifications of neodymium magnet

Two types of neodymium magnet were used for applying external field to the sample. Table 2.7 shows the specifications of each magnet.

Table 2.7 The specifications of Neodymium magnet

Neodymium magnet	1	2
Dimension [mm]	30 × 30 × 5	ϕ22 × 10
Maximum surface magnetic field value [T]	0.25	0.44
Maximum surface magnetic field value [T]	-0.12	-0.07

Moreover, Figure 2.4 and Figure 2.5 shows the result of one dimensional magnetic field distribution on the surface of each magnet (central part) using a Hall probe. The measurement was done by placing the Hall probe on the surface of the magnet (lift-off distance : 0.5 mm).

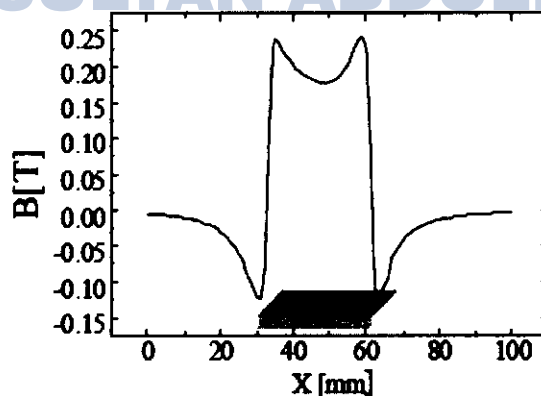


Figure 2.4 Surface magnetic field of neodymium magnet 1⁽⁴⁾.

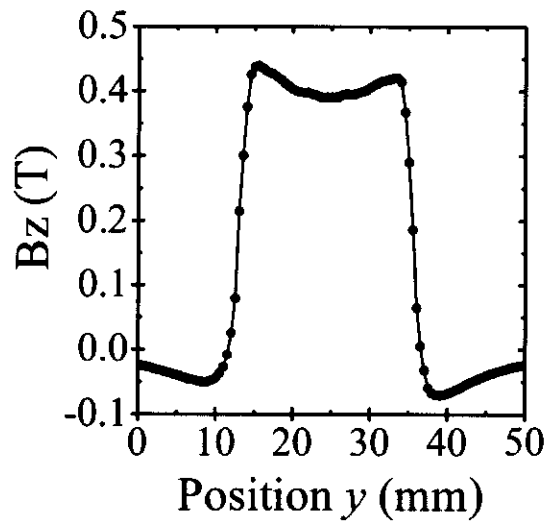


Figure 2.5 Surface magnetic field of neodymium magnet 2.

2.4.1.2 Magnetic field application method

Neodymium magnet that was used for applied magnetic field was set up at the backside of Hall probe. The strength of applied magnetic field at the detection part on Hall probe was calculated based on the stabilized Hall voltage that was detected on the surface of the Hall probe. Table 2.8 shows the value of the applied magnetic field. However, 2 magnets were used and pile up for neodymium magnet 2.

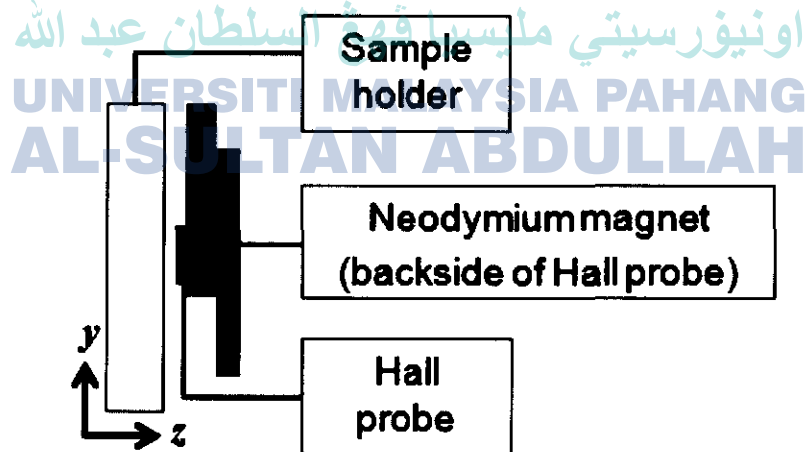


Figure 2.6 Magnetic field application method

Table 2.8 The applied magnetic field

Neodymium magnet	1	2
Hall probe surface magnetic field value [T]	0.14	0.33T

2.4.2 Lift-off distance

Lift-off distance, L is the distance between the Hall probe and the measurement sample. In this research, the magnetic field distribution measurement of the electrode mixed with iron wire was done by changing the lift-off distance into 0.5, 1.5, 2.5, 3.5 mm. Based on this result, the possible lift-off distance for the detection of magnetic field from iron particle was evaluated.

2.4.3 Measurement step

In this research, the magnetic field distribution measurement equipment, which two dimensional magnetic field distribution of the sample plane (x-y plane) is measured using a scanning Hall probe, was used. The measurement interval length was set to 0.2mm for both x and y direction. After the measurement starting point was decided, the measurement length and interval length were set up, and the magnetic field distribution of the sample was measured by the PC.

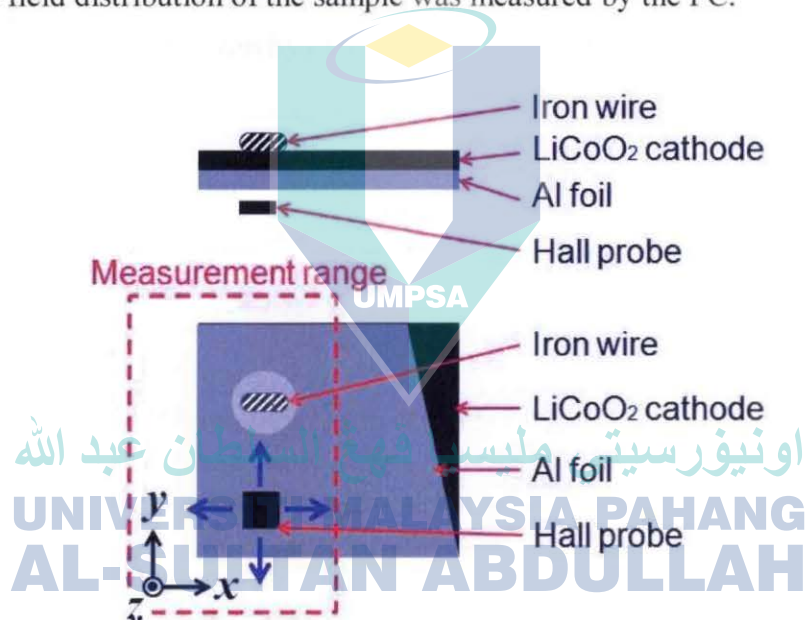


Figure 2.7 The outline diagram of measurement sample and magnetic field distribution measurement method

References

- (1) 酒井健司 : 「低温下でのグラファイト負極におけるリチウムデンドライト析出現象の観察および検知方法の検討」、豊橋技術科学大学修士学位論文 (2011)
Master thesis, Toyohashi University of Technology, (2011)
- (2) 香川智彦 : 「リチウムイオン電池用グラファイト負極におけるリチウムデンドライト析出現象の観察および検知」、豊橋技術科学大学修士学位論文 (2010)
Master thesis, Toyohashi University of Technology, (2010)
- (3) 篠原義和 : 「リチウムデンドライト析出現象における環境温度、電流密度依存性および析出検知方法の検討」、豊橋技術科学大学修士学位論文 (2010)
Master thesis, Toyohashi University of Technology, (2010)
- (4) 荒木優次 : 「走査ホール素子顕微鏡を用いた Bi2223 多芯ツイスト線材の均質性評価」、豊橋技術科学大学修士学位論文 (2008)
Master thesis, Toyohashi University of Technology, (2008)



اونيورسيتي مليسيا قهغ السلطان عبد الله
UNIVERSITI MALAYSIA PAHANG
AL-SULTAN ABDULLAH

CHAPTER 3

Study on Magnetic Field Distribution of Electrode with Iron Wire

3.1 Introduction

Previous chapter is focused on the preparation procedure of the sample and the magnetic field distribution measurement method. This chapter shows the magnetic field distribution measurement results for the prepared sample. From the result, this chapter discusses whether the change in the detected magnetic field from the measurement sample, which is the electrode mixed with iron wire as metallic contaminant, depend on dimension size (diameter and length) of iron wire and lift-off distance. In addition, the necessary condition for measurement of the magnetic field distribution from iron particle, which describe in Chapter 5, is also discussed.

3.2 Magnetic field distribution of electrode with iron wire with different diameter

The magnetic field distribution measurement of the electrode mixed with a small piece of iron wire, which the preparation of it is described in Chapter 2, was carried out at 0.14T applied magnetic field.

First of all, the result for the magnetic field distribution (two dimensional and one dimensional) of the electrode mixed with iron wire, when the length of iron wire is fixed to 1mm and diameter is 20, 50, 70, 100 μ m, is shown in Figure 3.1 until Figure 3.8 respectively. Here, the strength of magnetic field B_z is plotted by subtracting the detected magnetic field from the applied magnetic field on Hall probe surface (0.14T).

Based on one dimensional field distribution result for each sample shows when the lift off distance is increased, the detected magnetic field peak value is decreased monotonously. On the other hand, it can be confirmed that the magnetic field distribution that generated from iron wire can be observed and the change of area is growing with increasing lift-off distance.

3.2.1 Iron wire with diameter 100 μ m and length 1mm

The result of the two-dimensional magnetic field distribution of electrode mixed with iron wire with diameter of 100 μ m and length 1mm is shown in Figure 3.1. From this figure, the change of magnetic field distribution can be detected in the area of iron wire caused by the magnetization of iron wire. In addition, Figure 3.2 shows the one-dimensional magnetic field distribution along y direction when fixing the value of x, $x = 6.0 - 7.2$ mm.

3.2.2 Iron wire with diameter 70 μ m and length 1mm

The result of the two-dimensional magnetic field distribution of electrode mixed with iron wire with diameter of 70 μ m and length 1mm is shown in Figure 3.3. From this figure, the change of magnetic field distribution can be detected in the area of iron wire caused by the magnetization of iron wire. In addition, Figure 3.4 shows the one-dimensional magnetic field distribution along y direction when fixing the value of x, $x = 5.0 - 6.2$ mm.

3.2.3 Iron wire with diameter 50 μ m and length 1mm

The result of the two-dimensional magnetic field distribution of electrode mixed with iron wire with diameter of 50 μ m and length 1mm is shown in Figure 3.5. From this figure, the change of magnetic field distribution can be detected in the area of iron wire caused by the magnetization of iron wire. In addition, Figure 3.6 shows the one-dimensional magnetic field distribution along y direction when fixing the value of x, $x = 5.6 - 6.4$ mm.

3.2.4 Iron wire with diameter 20 μ m and length 1mm

The result of the two-dimensional magnetic field distribution of electrode mixed with iron wire with diameter of 20 μ m and length 1mm is shown in Figure 3.7. From this figure, the change of magnetic field distribution can be detected in the area of iron wire caused by the magnetization of iron wire. In addition, Figure 3.8 shows the one-dimensional magnetic field distribution along y direction when fixing the value of x, $x = 5.0 - 6.6$ mm.

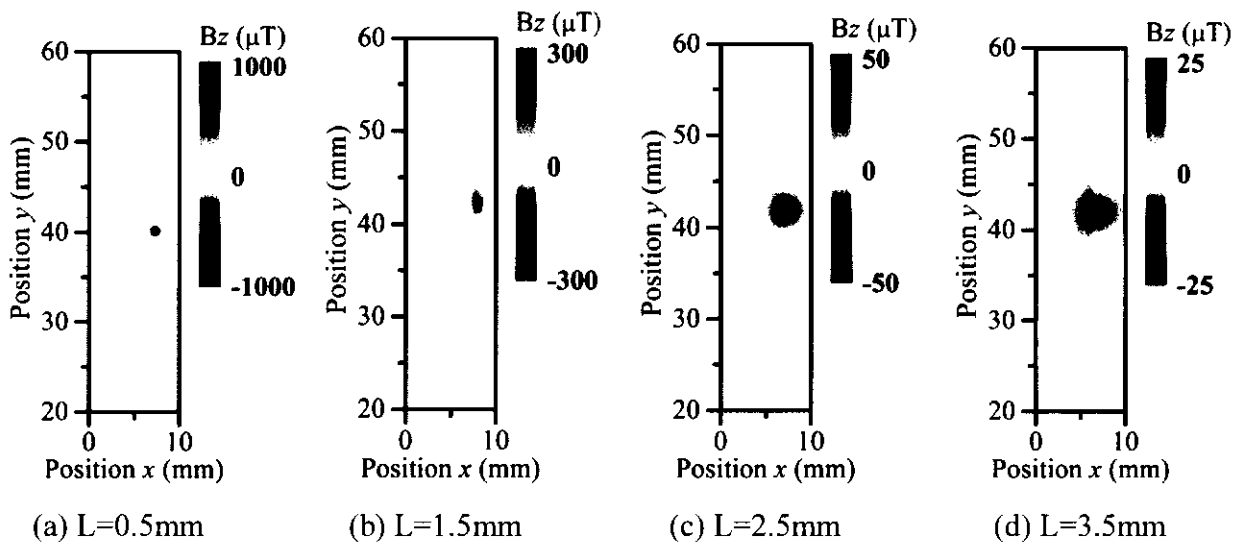


Figure 3.1 Two-dimensional magnetic field distribution of LiCoO_2 electrode with iron wire (diameter $100\mu\text{m}$, length 1mm) under applied magnetic field 0.14T

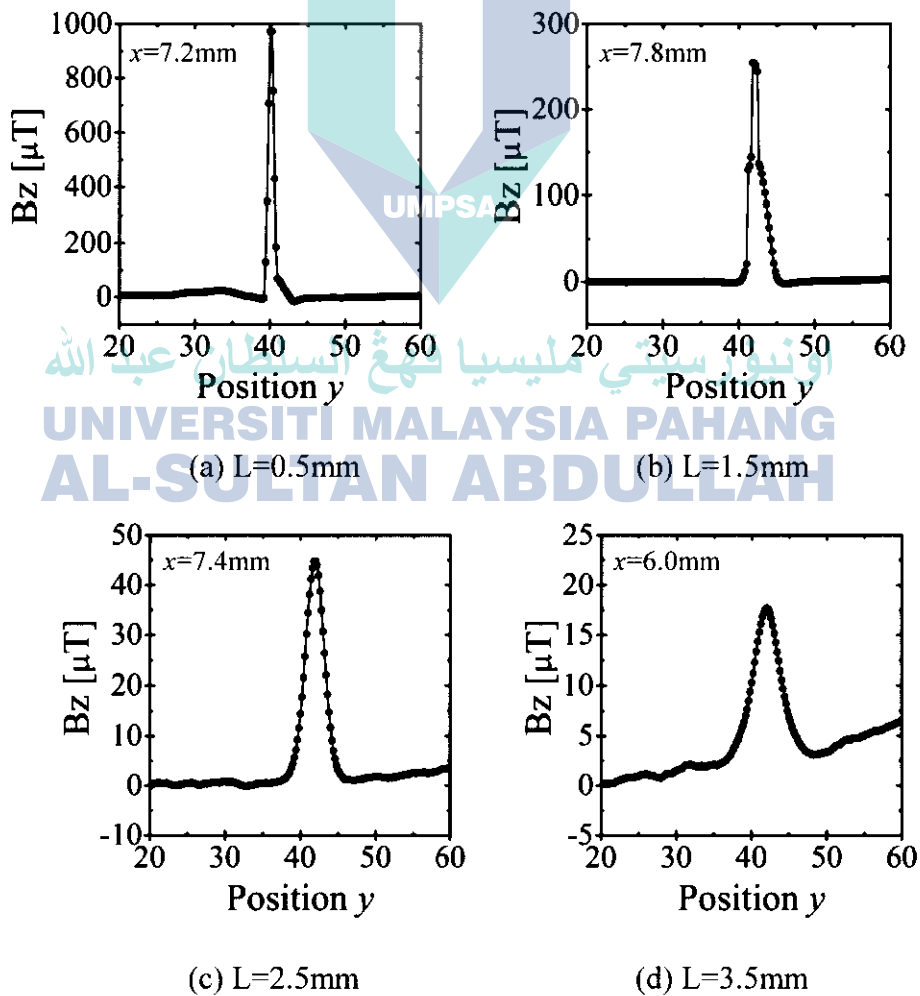


Figure 3.2 One-dimensional magnetic field distribution of LiCoO_2 electrode with iron wire (diameter $100\mu\text{m}$, length 1mm) under applied magnetic field 0.14T

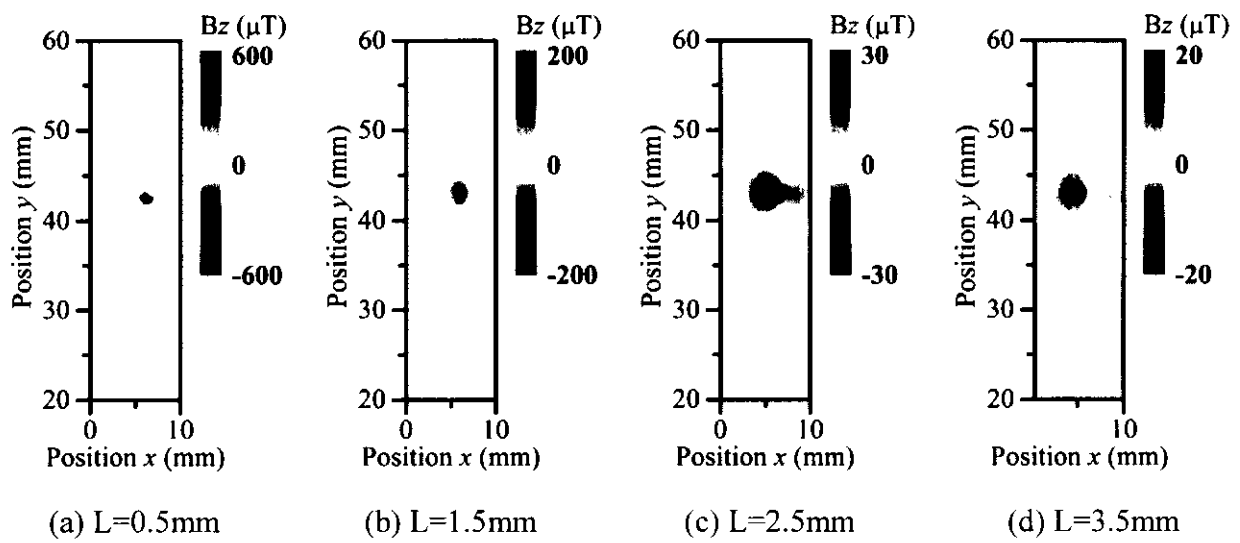


Figure 3.3 Two-dimensional magnetic field distribution of LiCoO_2 electrode with iron wire (diameter $70\mu\text{m}$, length 1mm) under applied magnetic field 0.14T

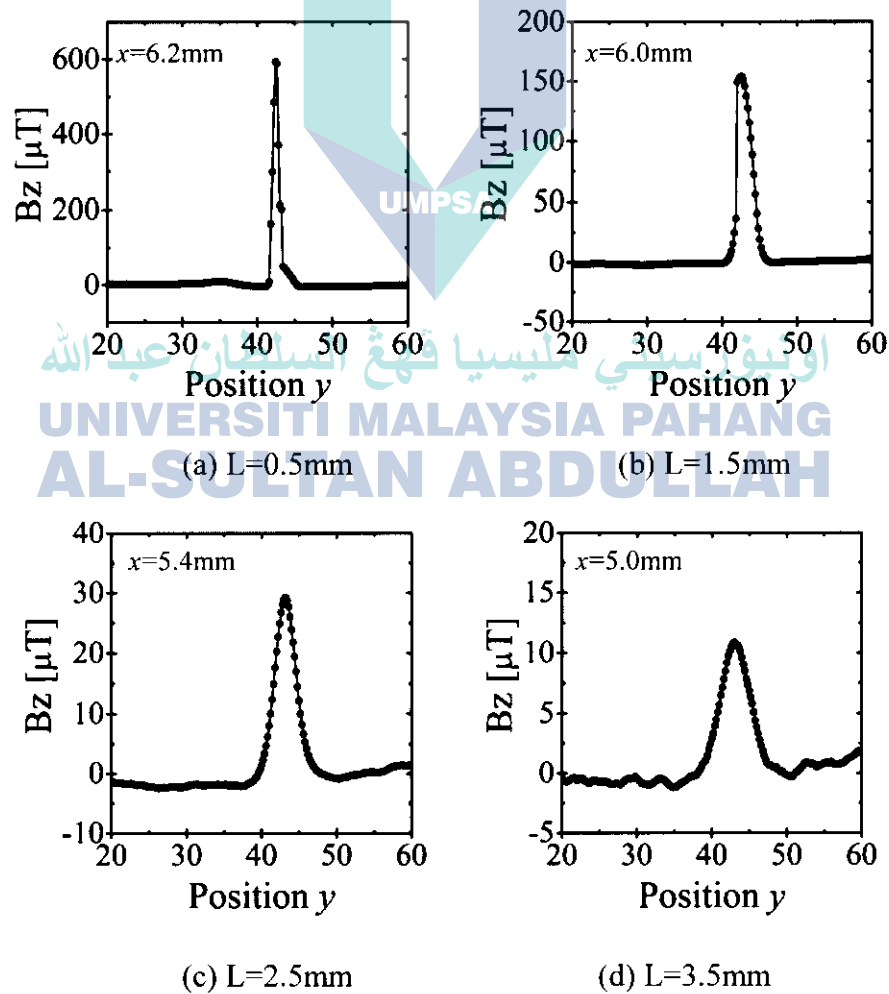


Figure 3.4 One-dimensional magnetic field distribution of LiCoO_2 electrode with iron wire (diameter $70\mu\text{m}$, length 1mm) under applied magnetic field 0.14T

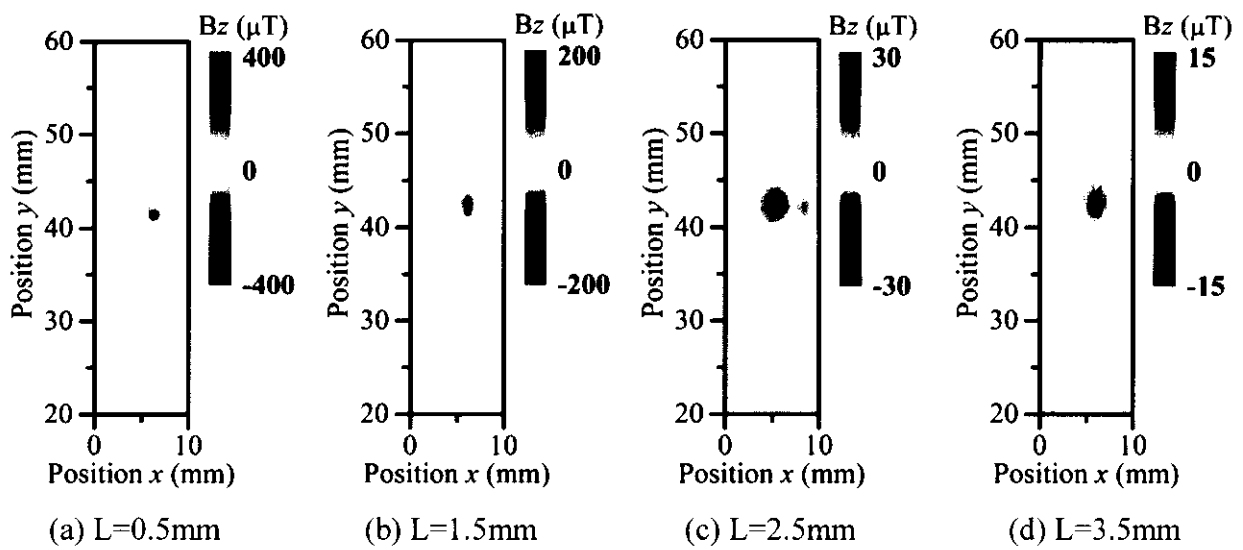


Figure 3.5 Two-dimensional magnetic field distribution of LiCoO₂ electrode with iron wire (diameter 50μm, length 1mm) under applied magnetic field 0.14T

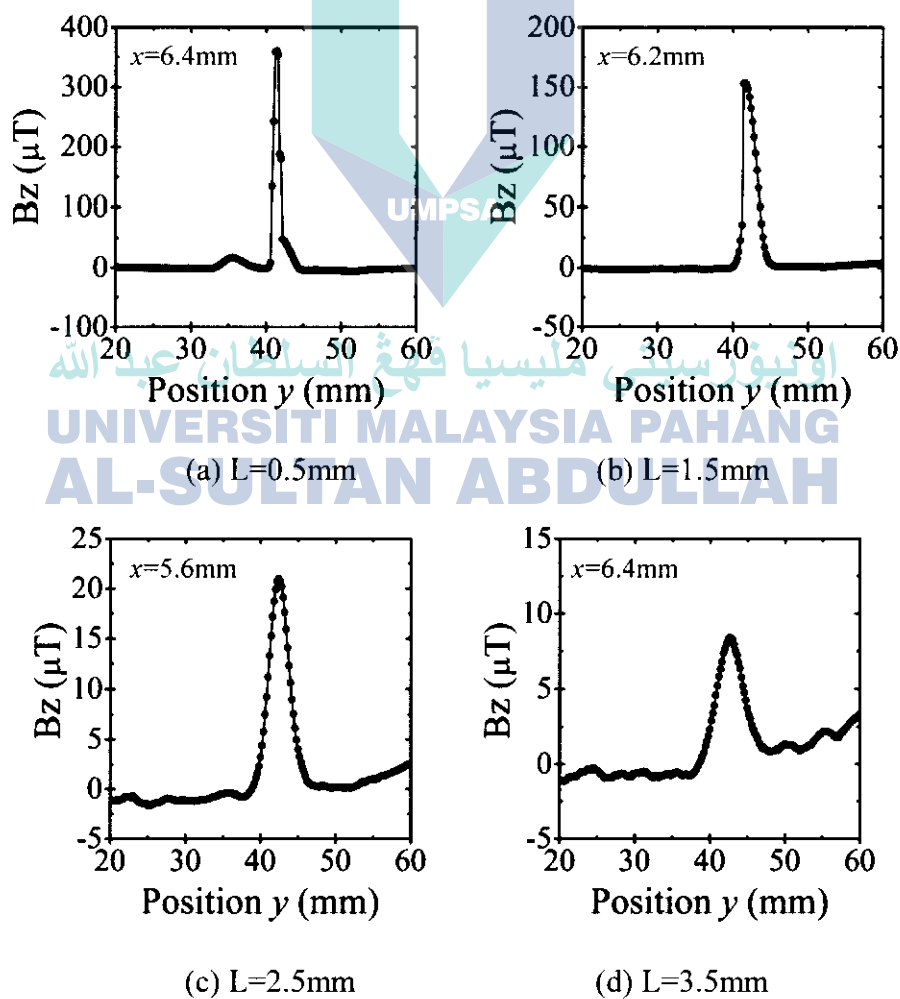


Figure 3.6 One-dimensional magnetic field distribution of LiCoO₂ electrode with iron wire (diameter 50μm, length 1mm) under applied magnetic field 0.14T

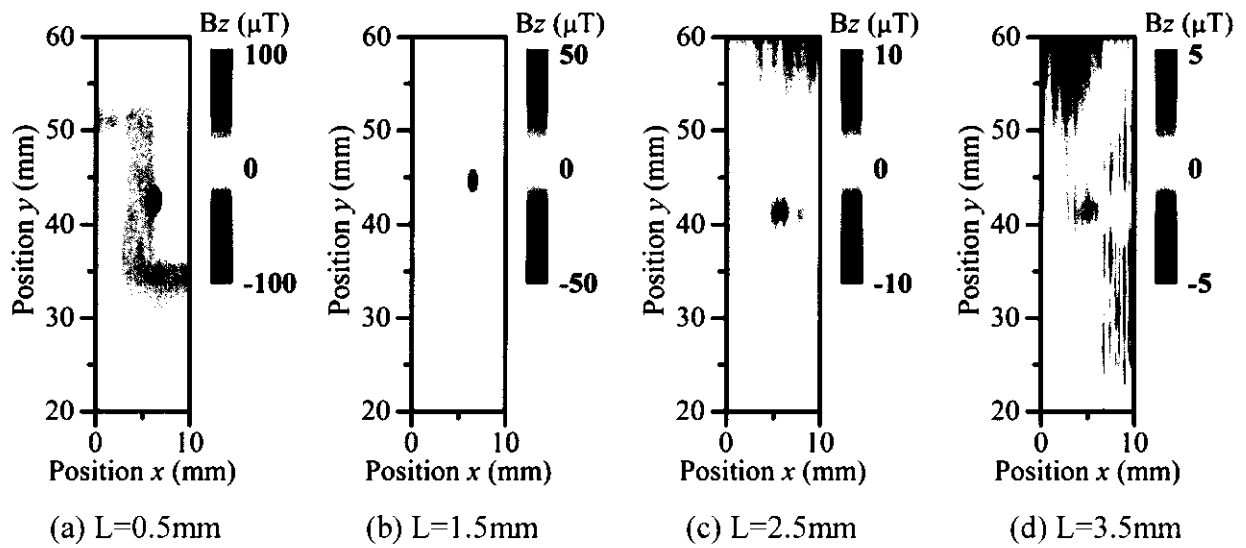


Figure 3.7 Two-dimensional magnetic field distribution of LiCoO_2 electrode with iron wire (diameter $20\mu\text{m}$, length 1mm) under applied magnetic field 0.14T

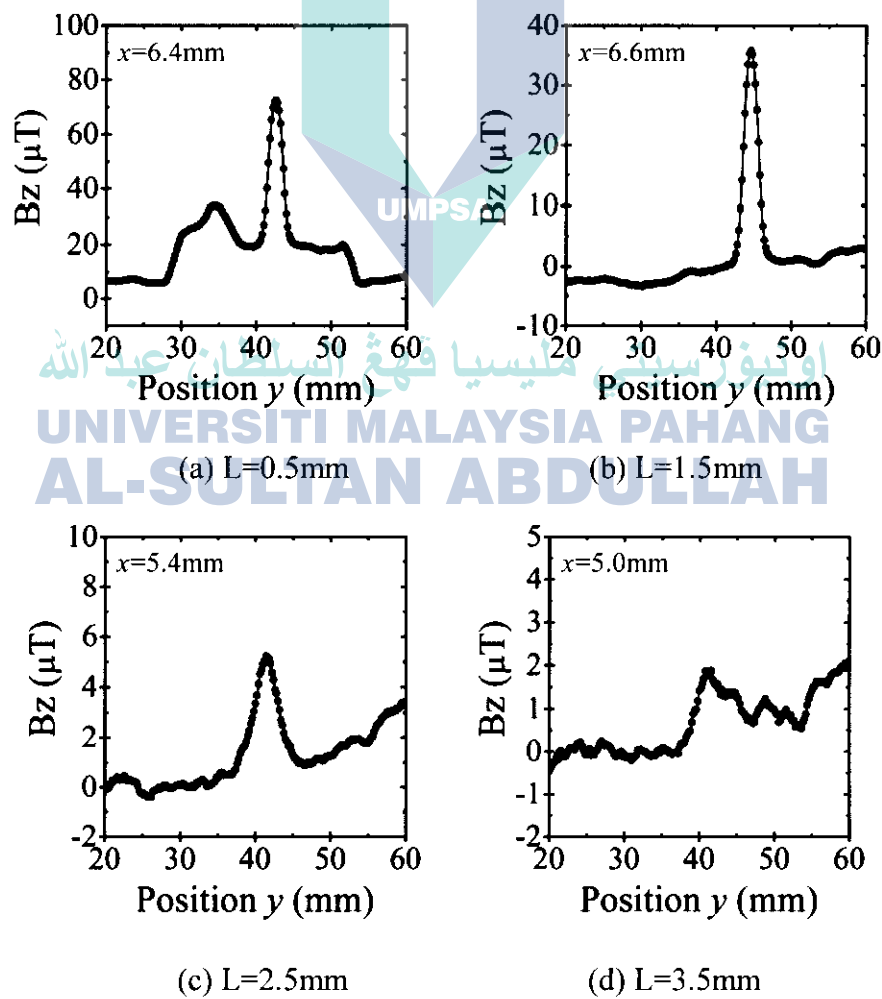


Figure 3.8 One-dimensional magnetic field distribution of LiCoO_2 electrode with iron wire (diameter $20\mu\text{m}$, length 1mm) under applied magnetic field 0.14T

3.2.5 Iron wire diameter and lift-off distance of magnetic field distribution dependence

When changing the diameter of iron wire and lift-off distance, detected magnetic field peak value B_z -max were compared for each condition as shown in Figure 3.9. From this, it is confirmed that B_z -max is monotonously decreased with the decreasing of iron wire diameter and also decreased with the increasing of lift-off distance. Furthermore, especially for the diameter of iron wire condition, B_z -max is proportional to the diameter of iron wire in the power of 1.5 can be observed.

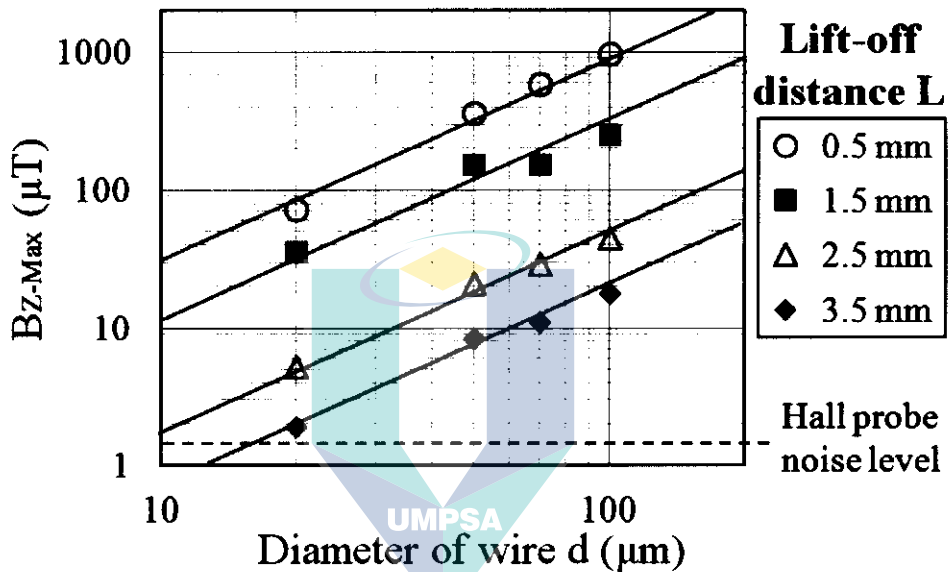


Figure 3.9 Diameter of iron wire and lift-off distance dependence of field peak value

3.2.6 Discussion on magnetic field distribution changed by lift-off distance

From Figure 3.1 - 3.8, it can be understood that when lift-off distance is increased, the half-value width of magnetic field distribution generated from iron wire is increased and the shape for magnetic field peak value became broader. This result shows increasing lift-off distance causes the strength of magnetic field can be detected decreased. However, as the magnetic field distribution of iron wire is appeared in more wide range, it can be suggested that even the metallic contaminant is not located directly below the Hall probe, magnetic field signal from it has the possibility to be detected.

3.3 Magnetic field distribution of electrode with iron wire with different length

Next, three kinds of iron wire which the diameter was fixed to $50\mu\text{m}$ and the length was changed in 0.5,1,2mm mixed in electrode as measurement sample and the magnetic field distribution measurement result (two-dimensional and one-dimensional) is shown in Figure 3.11-3.16. Here, the strength of magnetic field B_z is plotted by subtracting the detected magnetic field from the applied magnetic field on Hall probe surface (0.14T).

3.3.1 Iron wire with diameter $50\mu\text{m}$ and length 2mm

The result of the two-dimensional magnetic field distribution of electrode mixed with iron wire with diameter of $50\mu\text{m}$ and length 2mm is shown in Figure 3.11. From this figure, the change of magnetic field distribution can be detected in the area of iron wire caused by the magnetization of iron wire. In addition, Figure 3.12 shows the one-dimensional magnetic field distribution along y direction when fixing the value of x, $x = 4.6 - 5.2\text{mm}$.

3.3.2 Iron wire with diameter $50\mu\text{m}$ and length 1mm

The result of the two-dimensional magnetic field distribution of electrode mixed with iron wire with diameter of $50\mu\text{m}$ and length 1mm is shown in Figure 3.13. From this figure, the change of magnetic field distribution can be detected in the area of iron wire caused by the magnetization of iron wire. In addition, Figure 3.14 shows the one-dimensional magnetic field distribution along y direction when fixing the value of x, $x = 4.0 - 7.4\text{mm}$.

3.3.3 Iron wire with diameter $50\mu\text{m}$ and length 0.5mm

The result of the two-dimensional magnetic field distribution of electrode mixed with iron wire with diameter of $50\mu\text{m}$ and length 0.5mm is shown in Figure 3.15. From this figure, the change of magnetic field distribution can be detected in the area of iron wire caused by the magnetization of iron wire. In addition, Figure 3.16 shows the one-dimensional magnetic field distribution along y direction when fixing the value of x, $x = 4.2 - 5.0\text{mm}$.

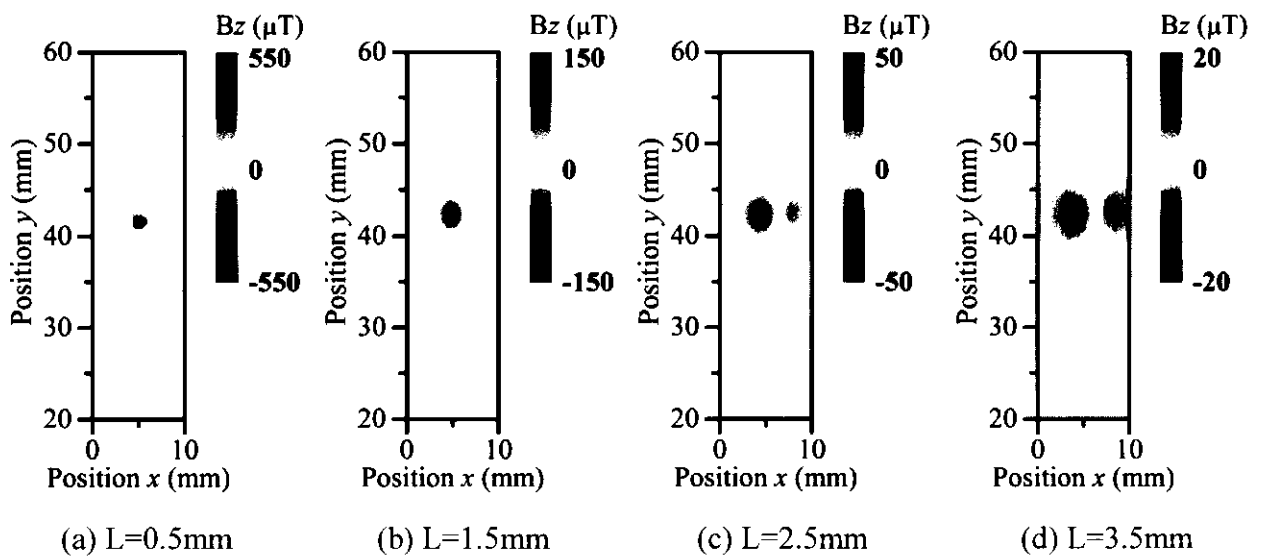


Figure 3.11 Two-dimensional magnetic field distribution of LiCoO_2 electrode with iron wire (diameter $50\mu\text{m}$, length 2mm) under applied magnetic field 0.14T

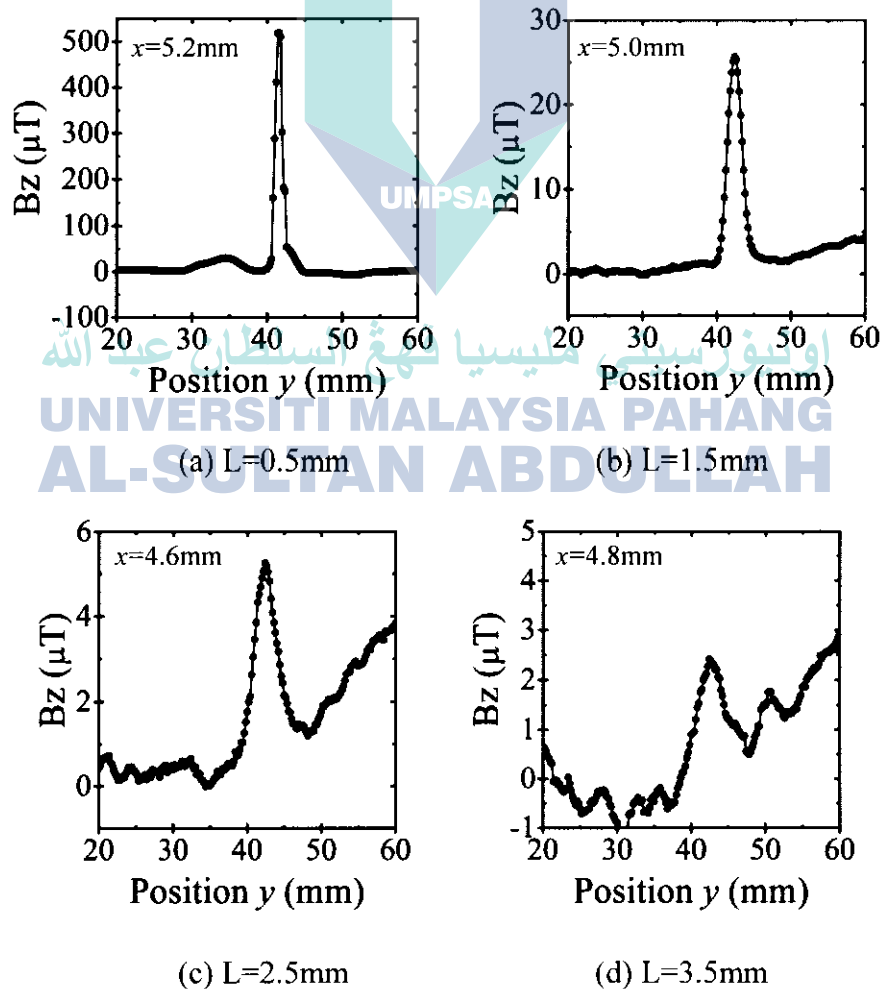


Figure 3.12 One-dimensional magnetic field distribution of LiCoO_2 electrode with iron wire (diameter $50\mu\text{m}$, length 2mm) under applied magnetic field 0.14T

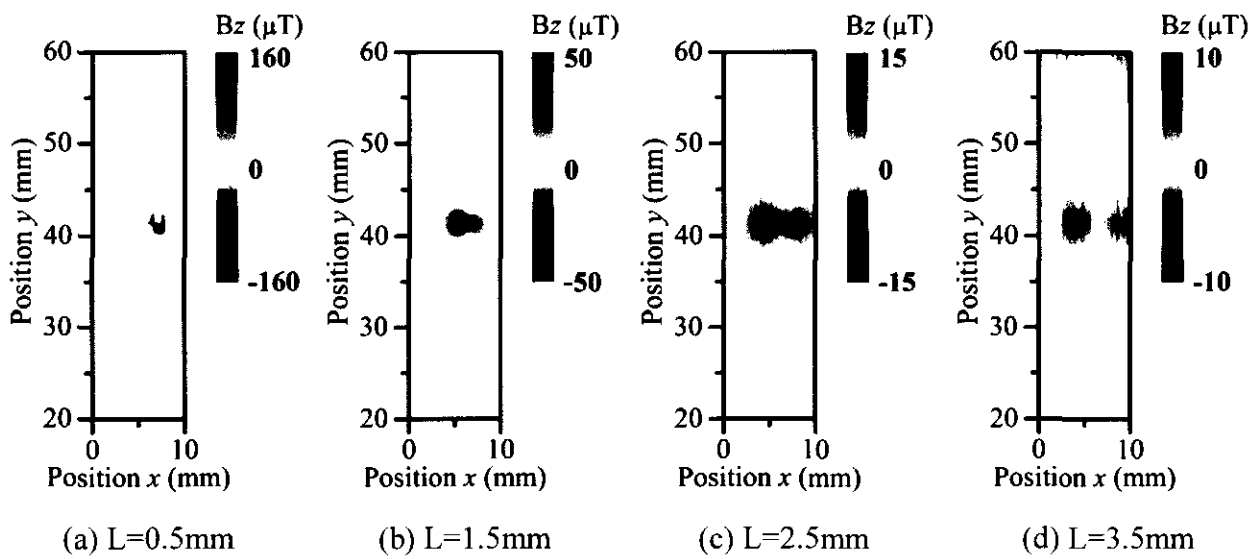


Figure 3.13 Two-dimensional magnetic field distribution of LiCoO_2 electrode with iron wire (diameter $50\mu\text{m}$, length 1mm) under applied magnetic field 0.14T

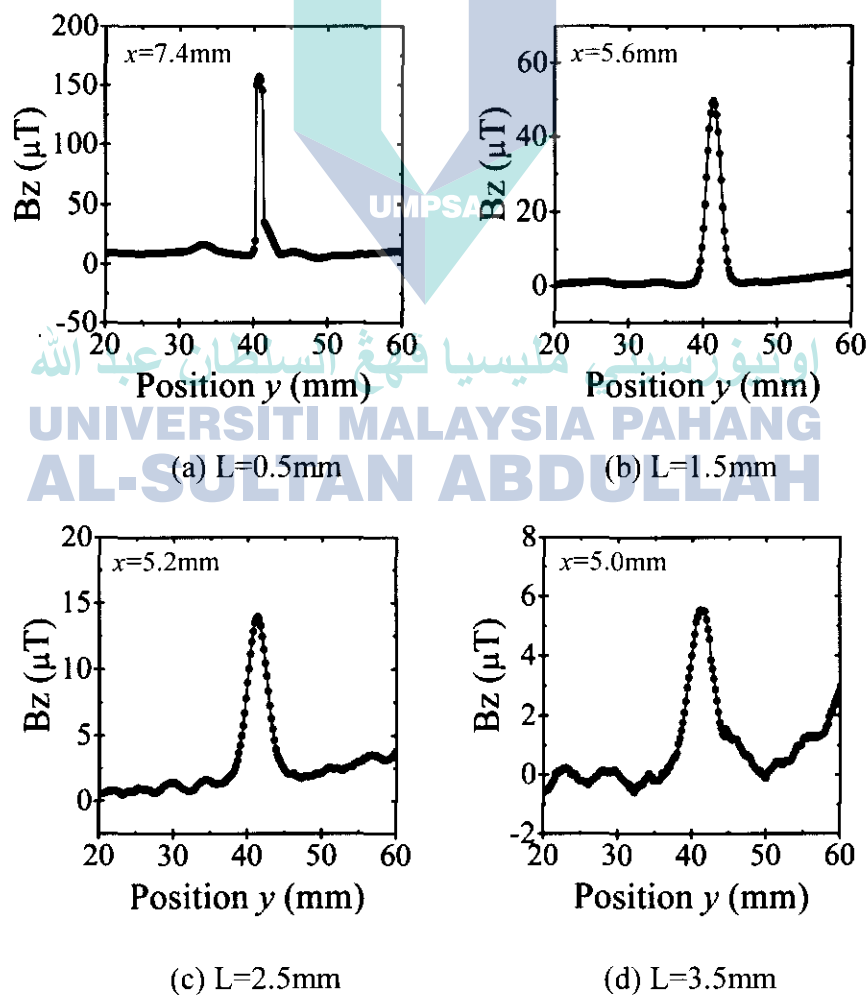


Figure 3.14 One-dimensional magnetic field distribution of LiCoO_2 electrode with iron wire (diameter $50\mu\text{m}$, length 1mm) under applied magnetic field 0.14T

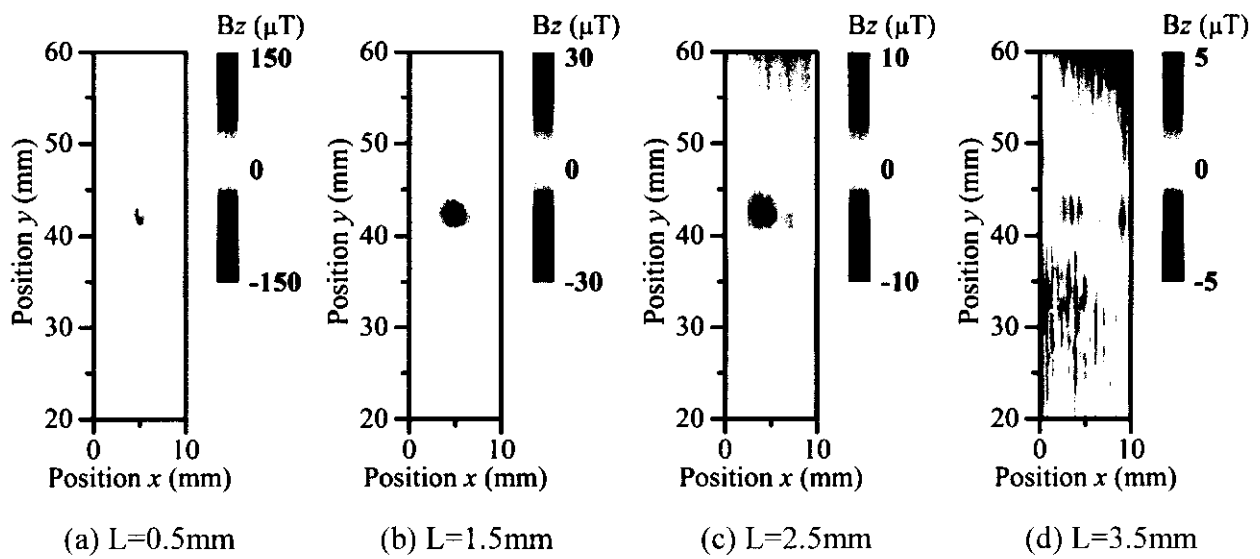


Figure 3.15 Two-dimensional magnetic field distribution of LiCoO_2 electrode with iron wire (diameter $50\mu\text{m}$, length 0.5mm) under applied magnetic field 0.14T

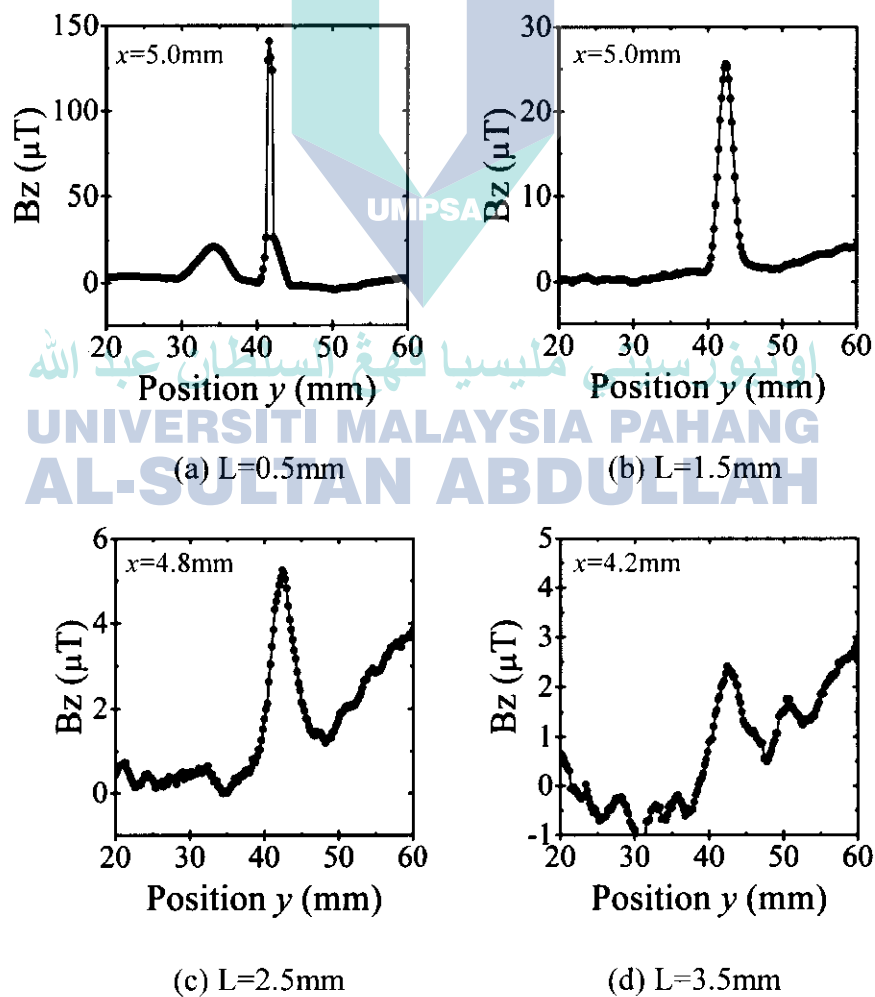


Figure 3.16 One-dimensional magnetic field distribution of LiCoO_2 electrode with iron wire (diameter $50\mu\text{m}$, length 0.5mm) under applied magnetic field 0.14T

3.3.4 The relation between wire length and field peak value

Detected magnetic field peak value $B_z\text{-max}$ obtained from Figure 3.11-3.16 is plotted against lift-off distance as shown in Figure 3.17. From this figure, it is confirmed $B_z\text{-max}$ is increased and decreased inversely proportional to the length of wire.

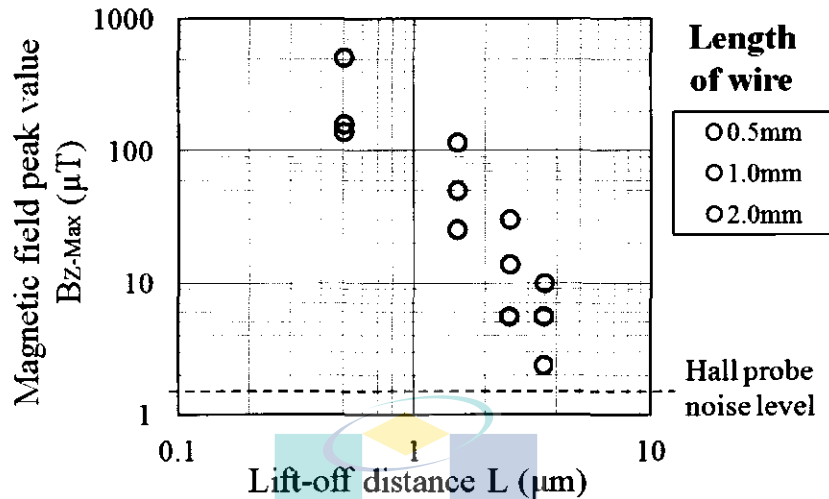


Figure 3.17 The relation between length of wire with diameter $50\mu\text{m}$ and field peak value

3.4 Discussion on magnetic field distribution measurement for electrode with iron particle

In case of fixing the diameter of iron wire, because of $B_z\text{-max}$ is inversely proportional to the wire length, and is increased and decreased had been confirmed, let consider iron particle with diameter of $50\mu\text{m}$ is almost similar to iron wire with diameter of $50\mu\text{m}$ and length of $50\mu\text{m}$, its $B_z\text{-max}$ is decreasing as illustrates by red frame in Figure 3.18 can be predicted. Thus, for electron mixed with iron particle with diameter of about $50\mu\text{m}$, lift-off distance has to be fixed to 1mm or less is suggested so that the magnetic field from iron particle can be detected.

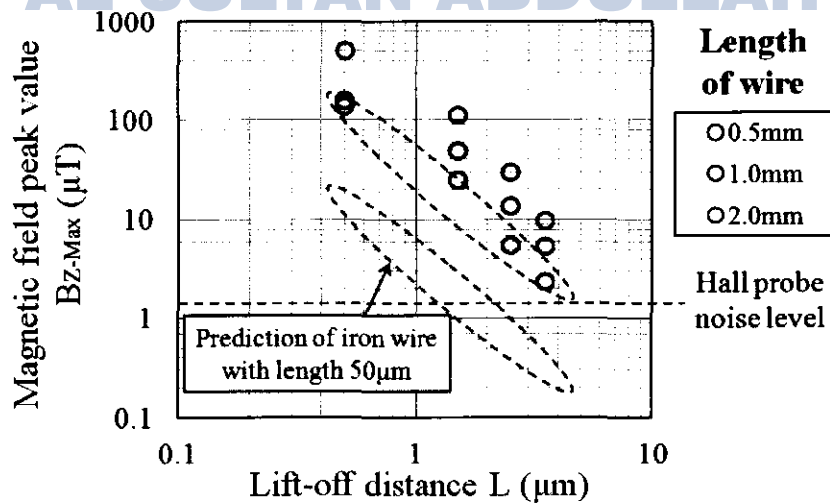


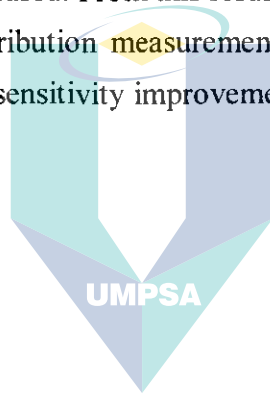
Figure 3.18 Prediction of magnetic field distribution of iron particle

CHAPTER 4

Study for Enhancing Measurement Sensitivity of Magnetic Field Distribution

4.1 Introduction

The magnetic field distribution measurement result of electrode with iron wire was shown in previous chapter. In case of electrode mixed with iron wire, the decreasing of iron wire dimension (diameter and length) would cause the decreasing of magnetic field distribution. This is also occurred when lift off distance is increased. From this result, to measure iron particle, it is necessary to enhancing the magnetic field distribution measurement sensitivity. This chapter describes the result of examining the measurement sensitivity improvement of magnetic field distribution.



اونيورسيتي مليسيا قهغ السلطان عبد الله
UNIVERSITI MALAYSIA PAHANG
AL-SULTAN ABDULLAH

4.2 Experimental procedure for enhancing measurement sensitivity

As described in Chapter 2, two Neodymium magnets were prepared as externally applied magnetic field. When each magnet was fixed at the back side of Hall probe, magnetic field detected by the detection part of Hall probe was corresponded to applied magnetic field. Chapter 3 showed the magnetic field distribution measurement result of electrode mixed with iron wire, which its diameter is $50\mu\text{m}$ and length is 1mm, under externally applied magnetic field 0.14T. Type and number of magnets was adjusted to increase the applied magnetic field for improvement of the magnetic field measurement sensitivity. The applied magnetic field was increased to 0.33T and the magnetic field measurement of electrode mixed with iron wire, which its diameter is $50\mu\text{m}$ and length is 1mm, was carried out under this condition. Then, the result under both condition of applied magnetic field 0.14T and 0.33T was compared to evaluate the improvement degree of magnetic field measurement sensitivity.

4.3 Measurement result

4.3.1 Applied magnetic field 0.14T

The result of the two-dimensional magnetic field distribution of electrode mixed with iron wire with diameter of $50\mu\text{m}$ and length 1mm under externally applied magnetic field 0.14T is shown in Figure 4.1. In addition, Figure 4.2 shows the one-dimensional magnetic field distribution along y direction when fixing the value of x, $x = 4.0 - 7.4\text{mm}$. From the result, the magnetic field from iron wire is able to be detected when lift off distance is 3.5mm and less.

4.3.2 Applied magnetic field 0.33T

The result of the two-dimensional magnetic field distribution of electrode mixed with iron wire with diameter of $50\mu\text{m}$ and length 1mm under externally applied magnetic field 0.33T is shown in Figure 4.3. In addition, Figure 4.4 shows the one-dimensional magnetic field distribution along y direction when fixing the value of x, $x = 5.0 - 5.6\text{mm}$. From the result, the magnetic field from iron wire is able to be detected when lift off distance is 3.5mm and less.

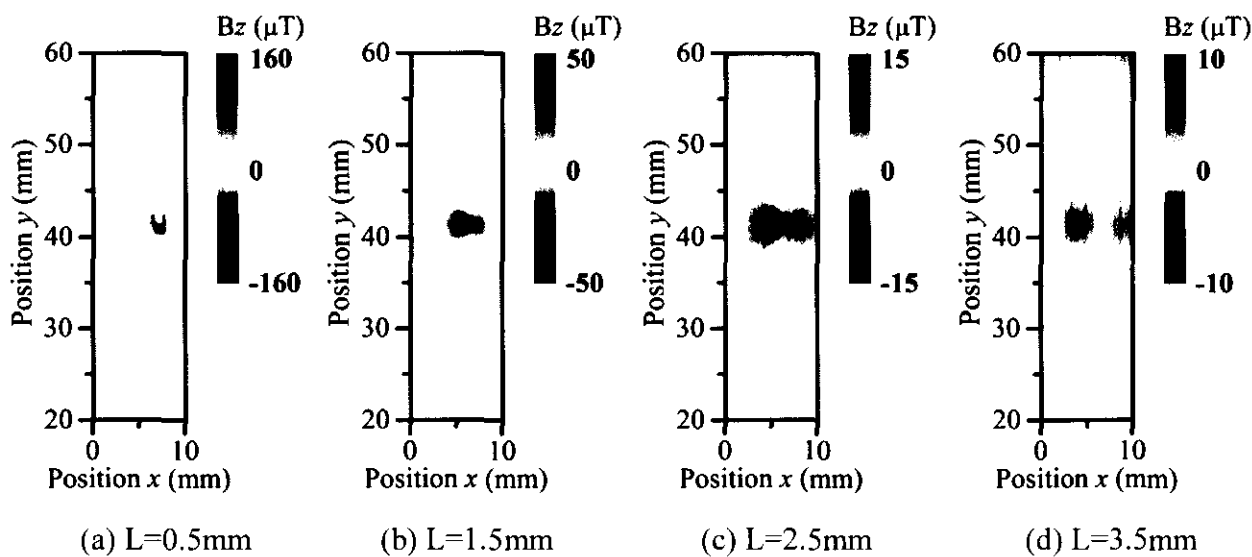


Figure 4.1 Two-dimensional magnetic field distribution of LiCoO_2 electrode with iron wire (diameter $50\mu\text{m}$, length 1mm) under applied magnetic field 0.14T

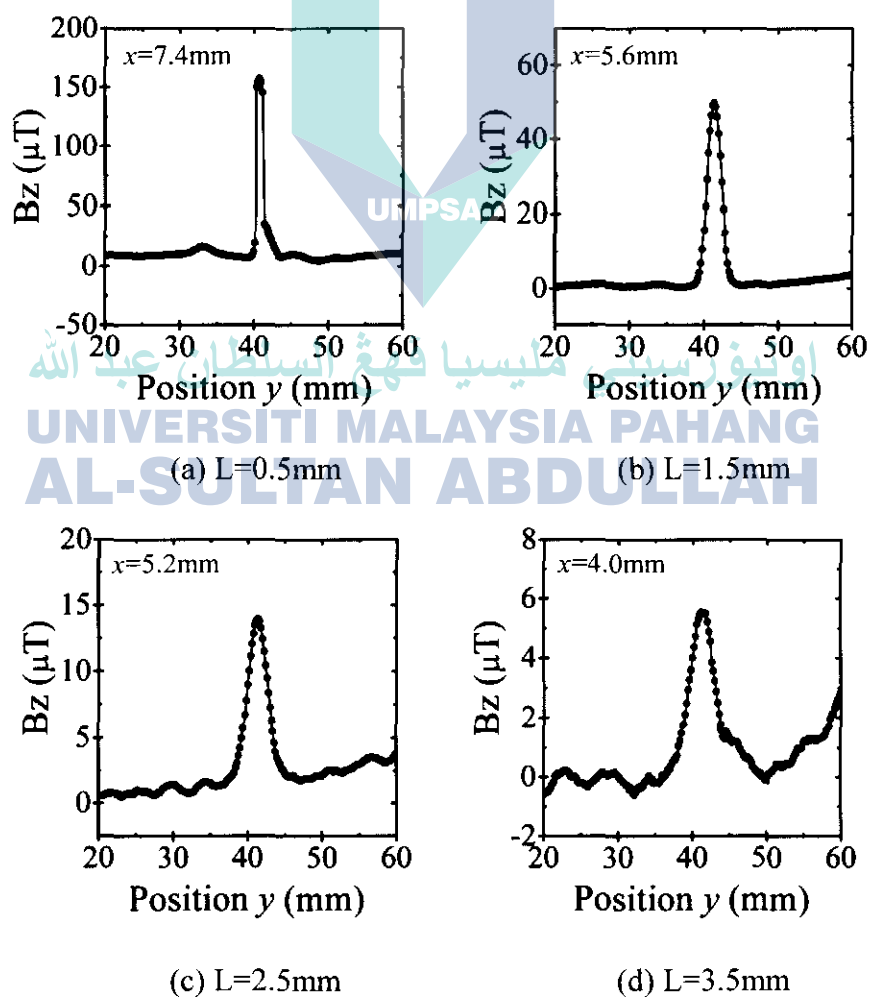


Figure 4.2 One-dimensional magnetic field distribution of LiCoO_2 electrode with iron wire (diameter $50\mu\text{m}$, length 1mm) under applied magnetic field 0.14T

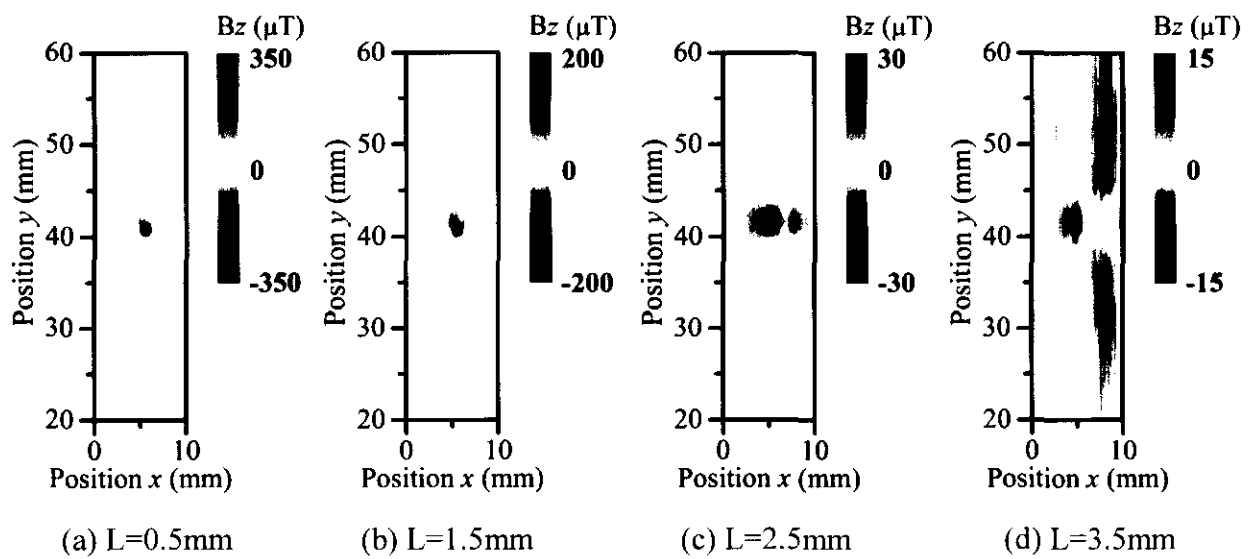


Figure 4.3 Two-dimensional magnetic field distribution of LiCoO_2 electrode with iron wire (diameter $50\mu\text{m}$, length 1mm) under applied magnetic field 0.33T

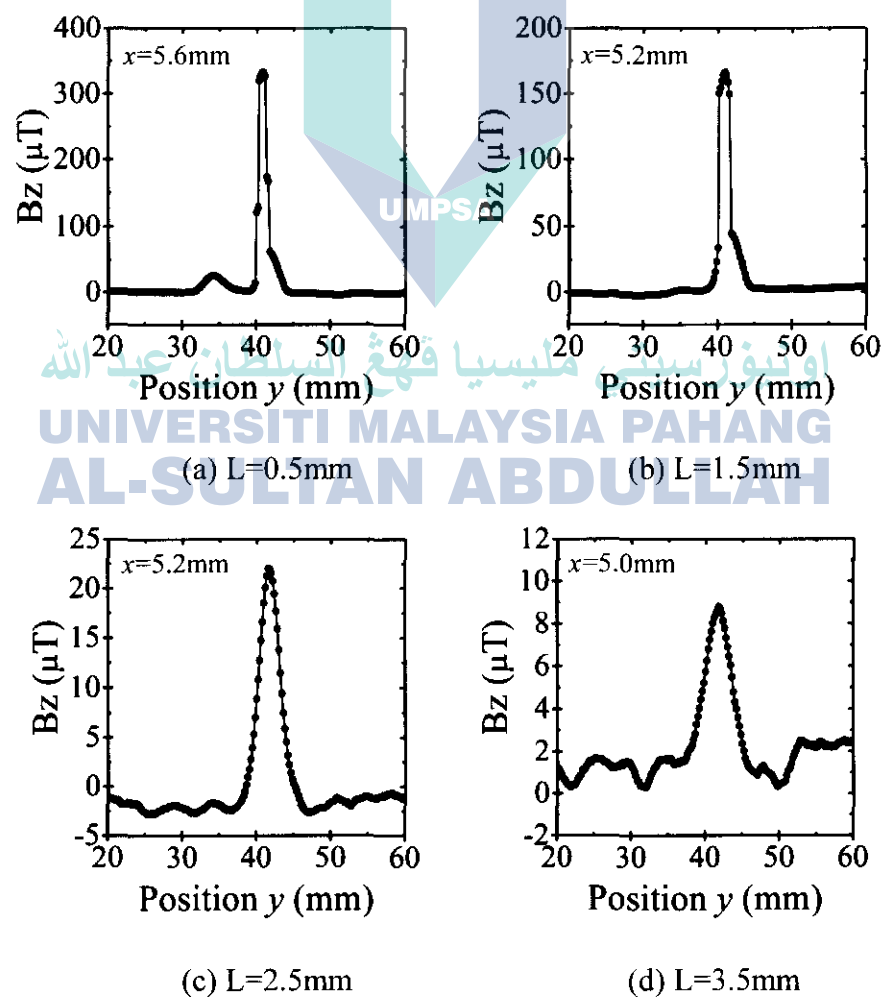


Figure 4.4 One-dimensional magnetic field distribution of LiCoO_2 electrode with iron wire (diameter $50\mu\text{m}$, length 1mm) under applied magnetic field 0.33T

4.3.3 Discussion on the effect of increasing applied magnetic field

The comparison result of detected magnetic field peak value B_z -max under both condition of applied magnetic field 0.14T and 0.33T is shown in Figure 4.5. From this figure, when the applied magnetic field is increase 2.4 times, the detected magnetic field peak value is increased double. It is thought that the magnetic field distribution measurement sensitivity can be improved by increasing the externally applied magnetic field.

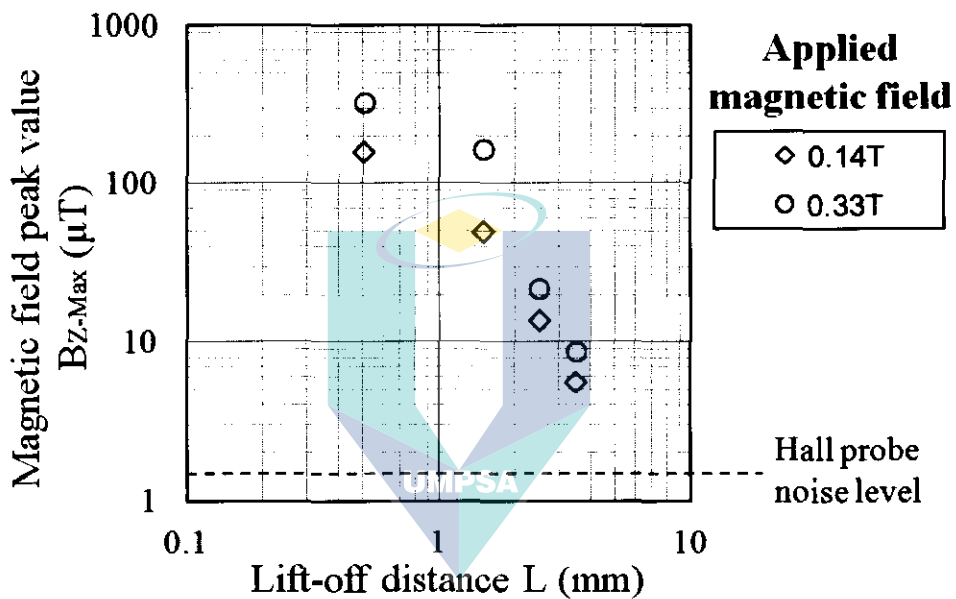


Figure 4.5 The change in magnetic field peak value of LiCoO_2 electrode with iron wire (diameter $50\mu\text{m}$, length 1mm) under applied magnetic field 0.14T and 0.33T

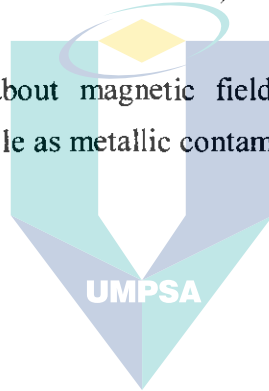
CHAPTER 5

Study on Magnetic Field Distribution of Electrode with Iron Particle

5.1 Introduction

In Chapter 3 and Chapter 4, the effect of changing iron wire dimension (diameter and length) and measurement condition (applied magnetic field strength and lift-off distance) to the result was discussed. Furthermore, based on the result, the estimation of necessary measurement condition (applied magnetic field strength and lift-off distance) for measuring iron particle with diameter about 50 μm was carried out.

This chapter shows the result about magnetic field distribution of electrode mixed with 50-100 μm diameter size of iron particle as metallic contaminant.



اونيورسيتي مليسيا قهغ السلطان عبد الله
UNIVERSITI MALAYSIA PAHANG
AL-SULTAN ABDULLAH

5.2 Magnetic field distribution measurement of electrode with iron particle with different diameter

The sample of electrode mixed with a piece of iron particle was prepared as described in Chapter 2 and then the magnetic field distribution of the sample was carried out. Based on discussion in Chapter 3 and Chapter 4, magnetic field measurement for iron particle was carried out under the condition of 0.5mm lift-off distance and 0.33T externally applied magnetic field.

5.2.1 Iron particle with diameter 80 μm

5.2.1.1 SEM image

Figure 5.1 shows the SEM image of the iron particle with diameter size 80 μm . The shape of iron particle is flat-shape can be observed from the image.

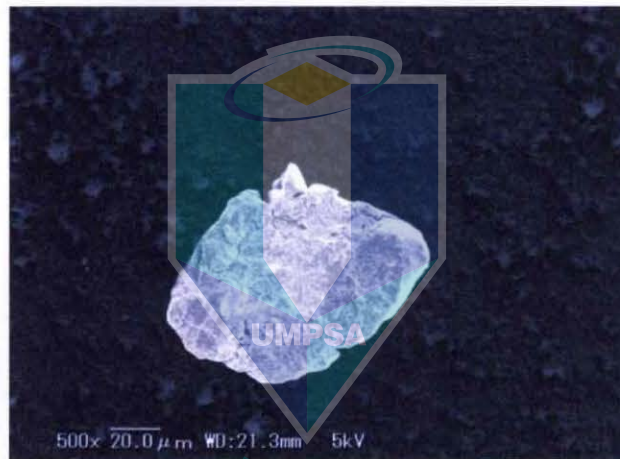


Figure 5.1 SEM image of iron particle with diameter size 80 μm

5.2.1.2 Magnetic field distribution measurement result

Magnetic field distribution measurement result is shown in Figure 5.2 for a flat-shaped iron particle with diameter 80 μm and in Figure 5.3 for electrode mixed with the same iron particle as a metallic contaminant. In case of measuring single iron particle only, magnetic field generated from the magnetization of iron particle as correspond to the magnetic field distribution can be detected. On the other hand, in case of measuring electrode mixed with iron particle, field generated from iron particle and also near the area of electrode edge was detected. If the iron particle is mixed into the electrode edge area, the possibility for this metallic contaminant to be detected becoming difficult suggested. In addition, the generation factor of magnetic field from electrode is discussed later in 5.3.

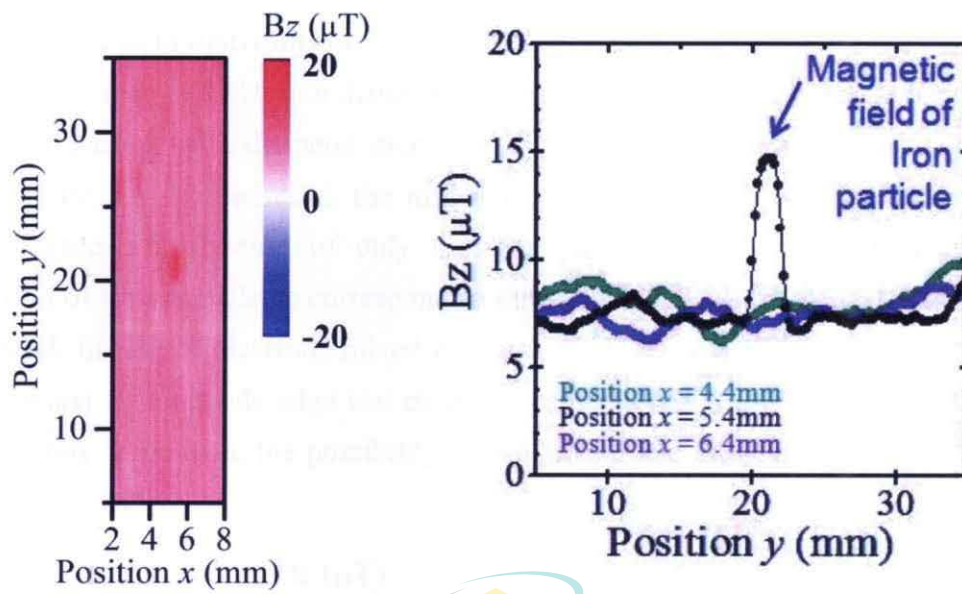


Figure 5.2 Magnetic field distribution of flat-shaped iron particle with diameter 80µm

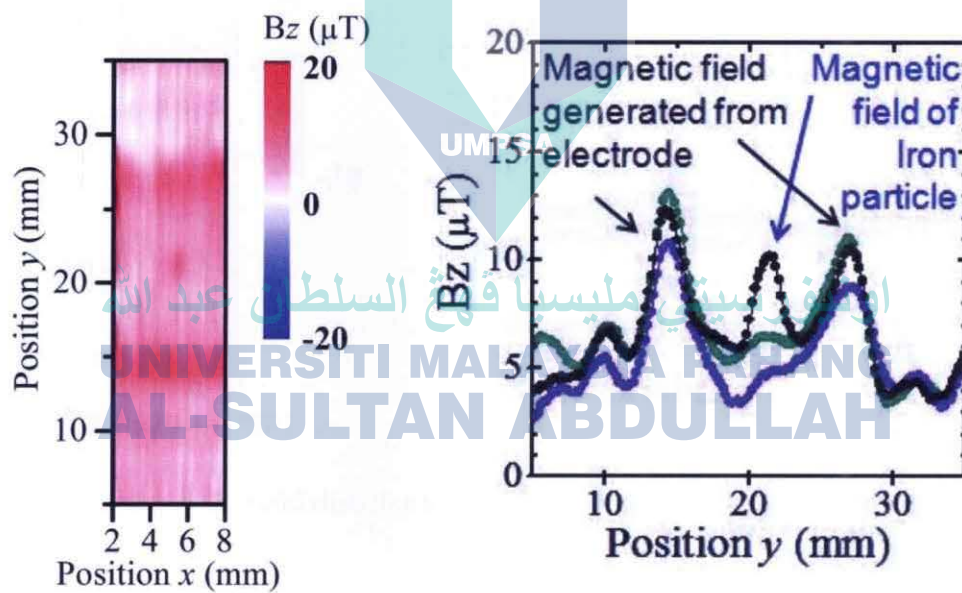


Figure 5.3 Magnetic field distribution of electrode with iron particle with diameter 80µm

5.2.2 Iron particle with diameter more than 100 μm

5.2.2.1 Magnetic field distribution

Two pieces of iron particle with diameter 80 μm were picked up and arranged side to each other to imitate iron particle with diameter more than 100 μm and the magnetic field distribution of it is shown in Figure 5.4. Furthermore, the magnetic field distribution of electrode mixed with it is shown in Figure 5.5. In case of only the iron particle, magnetic field generated from the magnetization of iron particle as correspond to the magnetic field distribution can be detected. On the other hand, in case of electrode mixed with iron particle, field generated from iron particle and also near the area of electrode edge was detected as mentioned before. If the iron particle is mixed into the electrode edge area, the possibility for this metallic contaminant to be detected becoming difficult is suggested.

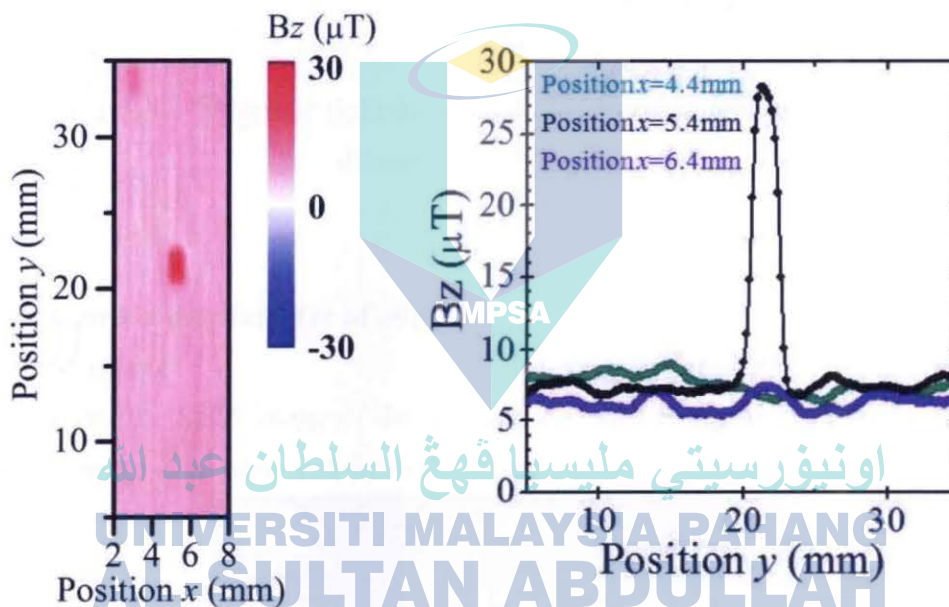


Figure 5.4 Magnetic field distribution of iron particle with diameter more than 100 μm

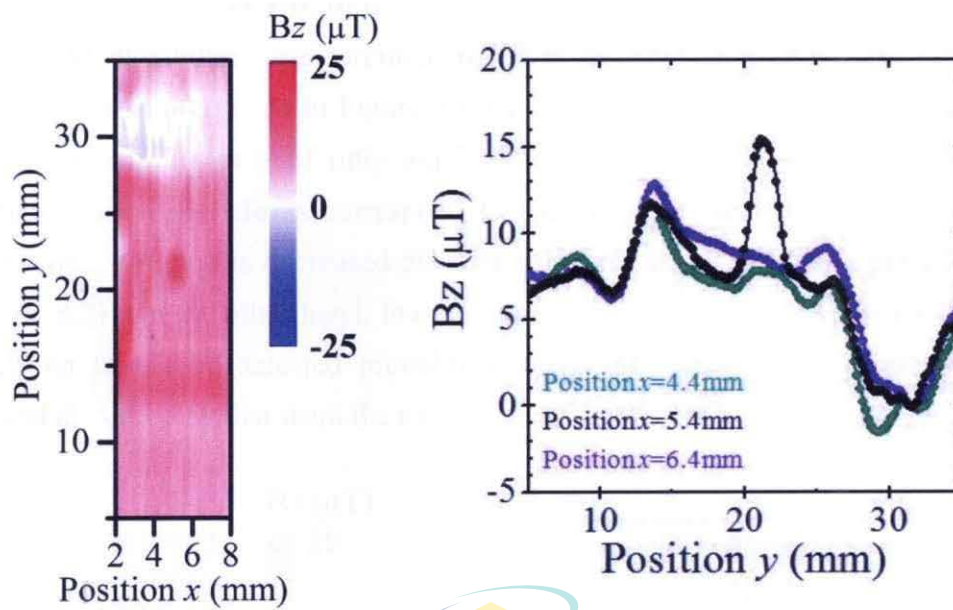


Figure 5.5 Magnetic field distribution of electrode with iron particle with diameter more than 100µm

5.2.3 Iron particle with diameter of 60µm

5.2.3.1 SEM image

Figure 5.6 shows the SEM image of the iron particle with diameter size 60µm. The shape of iron particle is flat-shape can be observed from the image.

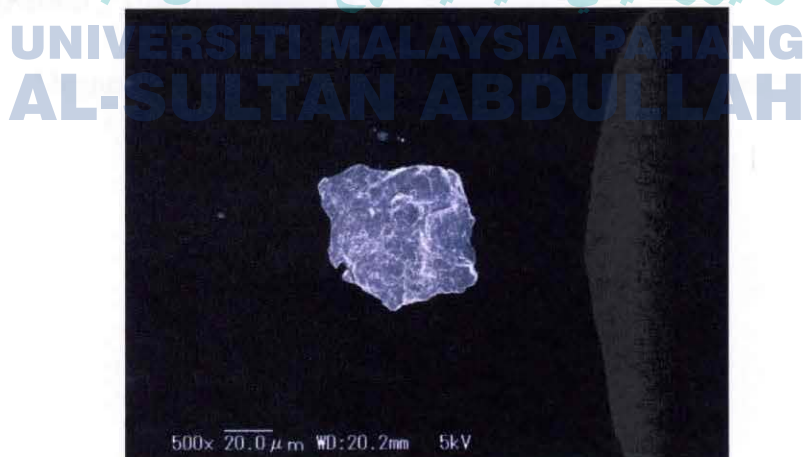


Figure 5.6 SEM image of iron particle with diameter size 60µm

5.2.3.2 Magnetic field distribution

Magnetic field distribution measurement result is shown in Figure 5.7 for a flat-shaped iron particle with diameter $60\mu\text{m}$ and in Figure 5.8 for electrode mixed with the same iron particle as a metallic contaminant. In case of only single iron particle, magnetic field generated from the magnetization of iron particle as correspond to the magnetic field distribution can be detected, however, the field strength is decreased 50-60% compared to result of iron particle with diameter $80\mu\text{m}$ (Figure 5.2). On the other hand, in case of electrode mixed with iron particle, the field from iron particle could not be detected probably because the field strength from iron particle was decreased and disturbed by that from the electrode.

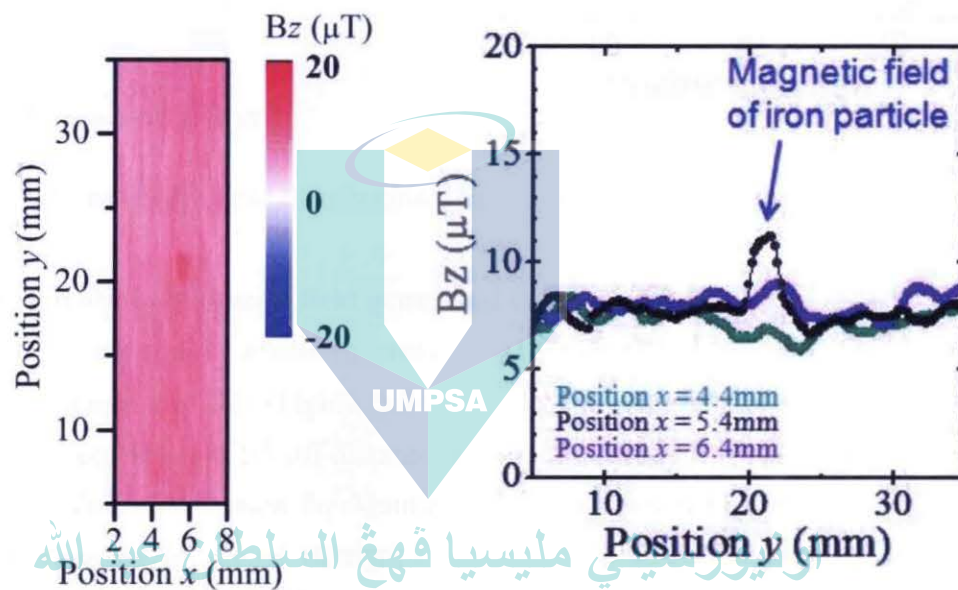


Figure 5.7 Magnetic field distribution of flat-shaped iron particle with diameter $60\mu\text{m}$

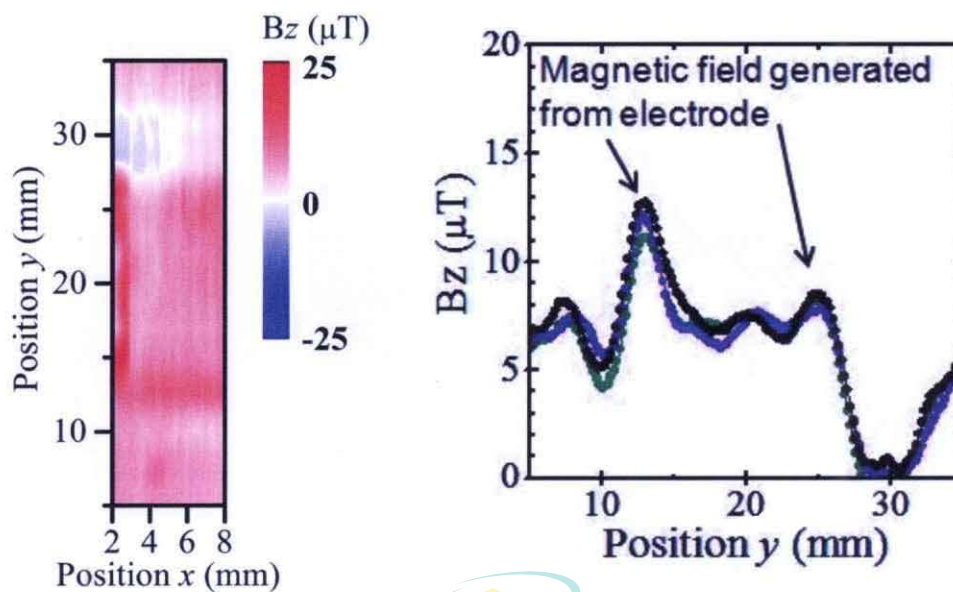


Figure 5.8 Magnetic field distribution of electrode with iron particle with diameter 60µm

5.3 Discussion about magnetic field generated from electrode

In case of consideration about magnetic field generated from electrode, the magnetic field distribution of aluminum foil (Figure 5.9) which is the material for preparing the electrode was measured under condition of lift off distance 0.5mm and externally applied magnetic field 0.33T.

The result of field distribution for Aluminum foil is shown in Figure 5.10. From figure, the field distribution obviously had equal strength to the magnetic field distribution that was thought to be from electrode in Figure 5.2-5.8 was observed. In addition, Energy Dispersive X-ray analysis (EDX) of Aluminum foil was carried out to check whether the magnetic field is generated by other element contained in Aluminum foil. The result is shown in Figure 5.11.



Figure 5.9 SEM image of Aluminum foil surface side for coating

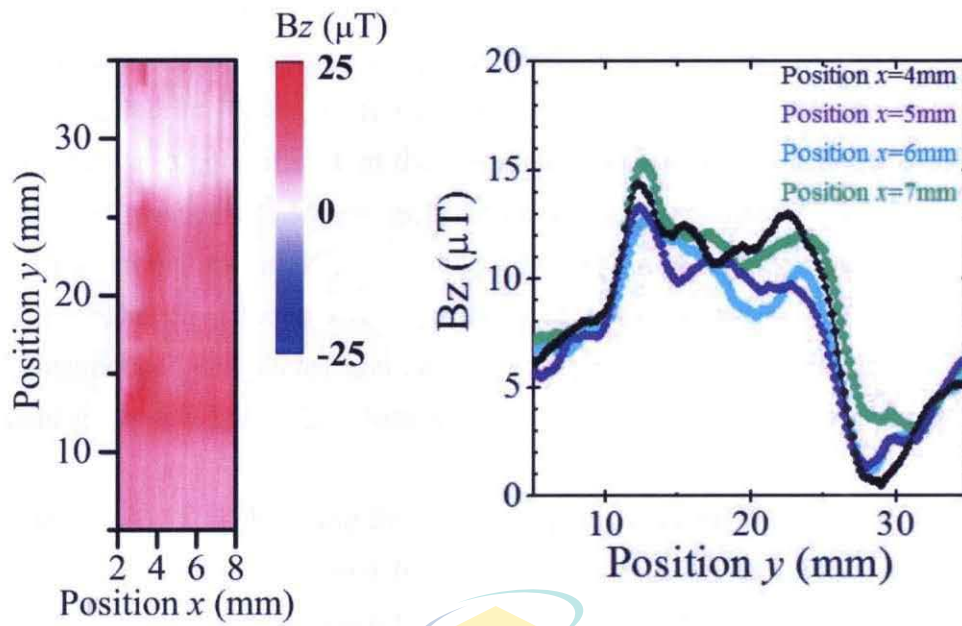


Figure 5.10 Magnetic field distribution on aluminum foil (coating side) at condition of $L=0.5\text{mm}$, applied magnetic field 0.33T

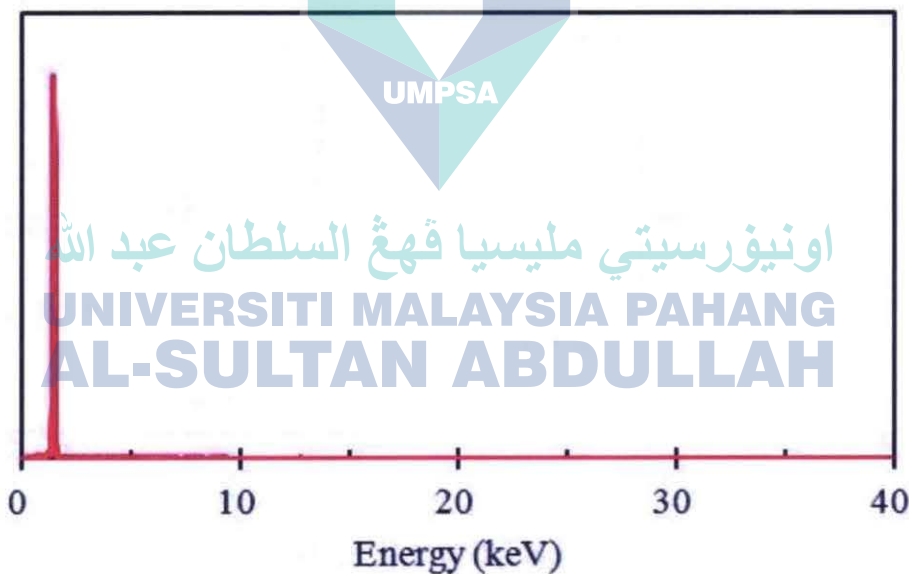


Figure 5.11 EDX result of Aluminum foil

A single peak can be observed at 1.49keV from Figure 5.11. The x-ray energy of Aluminum is $1.486\text{keV}^{(1)}$, therefore the obtained peak is originated from Al element and the result indicates other elements were not identified by EDX. From the result, there is high possibility that the reason the magnetic field was generated from Aluminum foil was due to electric and magnetic characteristic of Aluminum.

When magnetic field distribution is measured, the external magnetic field is also applied onto the Aluminum foil caused interlinkage magnetic field of it changed. In that case, based on the electromagnetic induction effect, eddy current flew in the metal of Aluminum foil was induced largely. Thus, there is a possibility that the magnetic field which was detected was generated from the induction of eddy current⁽²⁾. Moreover, Aluminum is a paramagnetic⁽³⁾, that does not magnetized when there is no external magnetic field and become weak magnetic when externally magnetic field is applied. As a result, it is thought the possibility of detected magnetic field was from aluminum that slightly magnetized. In this research, it is not possible to clarify which is the factor of detected magnetic field generated from aluminum and it is necessary to investigate the details about it in future.

On the other hand, when observing from the viewpoint to identify the magnetic field of metallic contaminant, magnetic field generated from aluminum foil acts as turbulence in the detection of field from metallic contaminant. Therefore, to reduce the influence of magnetic field originated from electrode, the adjustment of the direction of applied magnetic field and detected magnetic field of Hall probe as illustrated in Figure 5.12, and the improvement of magnetic field measurement sensitivity should be carried out. Furthermore, the study on the technology to shorten measurement time (as illustrated in Figure 5.13, the array of Hall probe) in the actual production line is essential.

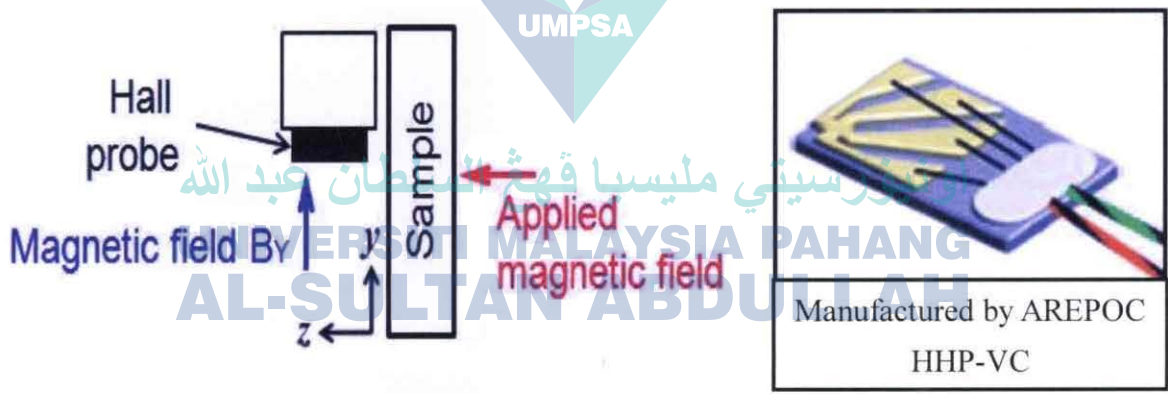


Figure 5.12 horizontal direction of magnetic field detection method (left) and The shape of Hall probe [4] (right)

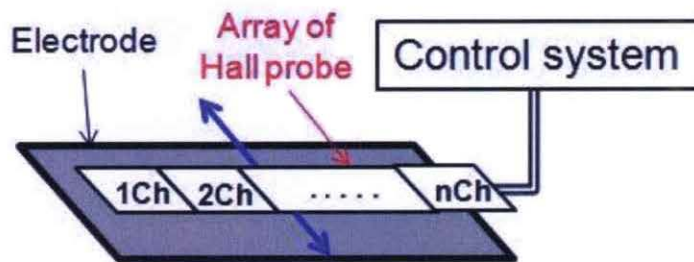
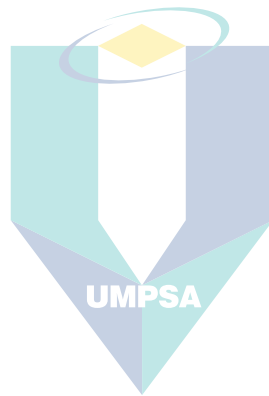


Figure 5.13 The array of Hall probe

References

- (1) X-ray Energy (keV) : <http://www.au-techno.com/edx1.html>
- (2) Eddy current : <http://denkinyumon.web.fc2.com/denkinokiso/uzudenryuu.html>
- (3) Aluminum : 小林 藤次郎 「アルミニウムのおはなし」日本規格協会
(Chapter 3, page 105) (1990)
- (4) Hall probe : <http://www.arepoc.sk/uploaded/download/HallProbes.PDF>
- (5) Richard L. Stoll : “The analysis of eddy currents” Oxford University Press (1974)



اونيورسيتي مليسيا قهغ السلطان عبد الله
**UNIVERSITI MALAYSIA PAHANG
AL-SULTAN ABDULLAH**

CHAPTER 6

Summary and Conclusion

In this research, we measured the magnetic field distribution of metallic contaminant in electrode for lithium-ion battery using Hall probe and examined the applicability for metallic contaminant detection technology that is more simple, easier and cheaper to replace the detection technology for metallic contaminant using X-ray inspection and high temperature superconductor SQUID device.

Chapter 1 explained the background, the objective and the outline of the research. Furthermore, the description about lithium ion battery such as the working principle, application, problem and the probability metallic contaminant mixed in electrode at production stage is described. The present detection technology of metallic contaminant, magnetic field measurement using Hall probe and others are also explained.

Experimental procedure is described in Chapter 2 where the preparation of measurement sample that are electrode and the one mixed with metallic contaminant, and the magnetic field distribution measurement procedure using Hall probe are explained.

Chapter 3 showed the study on magnetic field distribution of electrode mixed with iron wire. Iron wire with fixed length 1mm, and diameter was changed in 20, 50, 70 and 100 μ m was inserted into electrode as samples, and magnetic field distribution of samples was respectively measured under condition of 0.14T externally applied magnetic field and lift-off distance 0.5-3.5mm. The result indicates the change in magnetic field distribution was detected in the area of iron wire caused by the magnetization of iron wire. The detected magnetic field peak value tends to increase and decrease based on the change in wire diameter and lift-off distance was experimentally confirmed.

On the other hand, iron wire that diameter was fixed to 50 μ m and length was changed in 0.5, 1, 2mm was inserted into electrode and magnetic field distribution was respectively measured under same condition of 0.14T externally applied magnetic field and lift-off distance 0.5-3.5mm. As a result, the change in magnetic field distribution can be detected in the area of iron wire caused by the magnetization of iron wire. When diameter of iron wire was fixed, field peak value is increased and decreased inversely proportional to the length of iron wire.

Based on these results, in the case of iron particle with diameter size about $50\mu\text{m}$ was inserted into electrode, lift-off distance have to adjust to 1mm or less is suggested to this device for measuring magnetic field generated by iron particle that mixed in electrode.

In Chapter 4, the result of enhancing magnetic field distribution measurement sensitivity is shown. Iron wire with length 1mm and diameter $50\mu\text{m}$ was inserted into electrode, and the result of magnetic field distribution measured under condition of 0.33T externally applied magnetic field shows field peak value was increased double compared to measured under condition of 0.14T externally applied magnetic field. From the result mentioned above, measurement sensitivity could be improved by increasing externally applied magnetic field.

Chapter 5 showed the study on magnetic field distribution of electrode mixed with iron particle. Based on the results on Chapter 3 and Chapter 4, magnetic field distribution of flat-shaped iron particle with diameter $60\mu\text{m}$ and $80\mu\text{m}$ was respectively measured under condition of 0.33T externally applied magnetic field and lift-off distance 0.5mm. Magnetic field distribution of each iron particle that had been magnetized was measured.

On the other hand, when iron particle with diameter $80\mu\text{m}$ was inserted into electrode, magnetic field distribution of magnetized iron particle could be detected. As a result, the existence of iron particle with diameter $80\mu\text{m}$ in electrode can be identified. However, at the edge area of electrode, magnetic field distribution that assumed was originated from Aluminum foil was also detected, in the case of iron particle is mixed at that area, the detection of iron particle would become more difficult. Furthermore, in the case of iron particle with diameter $60\mu\text{m}$ was inserted into electrode, magnetic field distribution from magnetized iron particle was disturbed by that from the electrode. This result indicates the presence of iron particle with diameter $60\mu\text{m}$ in electrode could not be identified.

Finally, as for future task, to reduce the influence of magnetic field from electrode, the direction of detected magnetic field by Hall probe and the direction of externally applied magnetic field in measurement has to be adjusted for further improvement of measurement sensitivity. Furthermore, study on the technology (such as the array of Hall probe) to shorten measurement time in the actual production line is essential.

Acknowledgements

I wish to express my sincere gratitude to Associate Professor Ryoji Inada and Professor Yoji Sakurai, Department of Electrical Electronic and Information Engineering, Toyohashi University of Technology for the guidance and help from the beginning until the end to the accomplishment of this research and write this thesis.

I would like to sincerely appreciate Professor Shuichi Ichikawa and Associate Professor Yoshiyuki Suda, Department of Electrical Electronic and Information Engineering, Toyohashi University of Technology for examining my dissertation with beneficial discussion and suggestion.

Professors and Associate Professors of Electrical Systems Course, Department of Electrical Electronic and Information Engineering, Toyohashi University of Technology for the useful advice in preliminary dissertation.

Mr. Yoshihiko Hibi, Technical staff, Toyohashi University of Technology for the safety guidance.

I would like to deeply thank to My laboratory senior for the guidance of experimental procedure and more. Mr. Takayuki Tanaka, Mr. Kenta Shibukawa and Mr. Ryuta Ito; my laboratory members for the help and cooperation to the accomplishment of this research. Final-year master course students, first-year master course students and final-year degree course students; other laboratory members in Sakurai and Inada Laboratory

Finally, I wish to sincerely express my gratitude to My parents for the mentally support and encouragement during my student life. University of Malaysia, Pahang (UMP) for the financial support.

Research Achievement

Japan Internal Conference Presentation

1. ○Abdul Azim Jais, Ryoji Inada, Yoji Sakurai
“Detection of Metallic Contaminant in Electrode of Lithium Ion Battery Using Scanning Hall-probe Microscopy”
Tokai-Section Joint Conference on Electrical and Related Engineering 2012,
Toyohashi University of Technology, Japan,
24-25 September 2012.



اونيورسيتي مليسيا قهغ السلطان عبد الله
**UNIVERSITI MALAYSIA PAHANG
AL-SULTAN ABDULLAH**